Synthesis and Characterization of Semiconductor Nanostructures for Possible use in Photo-Splitting of Water

A synopsis of the proposed work
for the award of the degree

DOCTOR OF PHILOSOPHY
IN CHEMISTRY

Submitted by

Shailja Sharma

Forwarded

Prof. L.D. Khemani
Head, Dean
Dept. of Chemistry

Prof. Rohit Shrivastav
Advisor
Dept. of Chemistry

DEPARTMENT OF CHEMISTRY
FACULTY OF SCIENCE
DAYALBAGH EDUCATIONAL INSTITUTE
(DEEMED UNIVERSITY)
DAYALBAGH, AGRA-282 110
20th March, 2012

Synthesis and Characterization of Semiconductor Nanostructures for Possible use in Photo-Splitting of Water

OUTLINE

1. Solar – Hydrogen Generation by Photo-splitting of Water
2. Metal Oxide Semiconductors for PEC Splitting of Water
3. Layered/Core shell Nanostructures/Nanoarchitectures
4. Proposed Study
5. Objectives/Stages of the Proposed Work
6. Proposed Methodology
7. Tentative Plan of the Work
Annexure I: Literature Review

1. Solar – Hydrogen Generation by Photo-splitting of Water

The impending shortage of fossil fuels and environmental consequences of their consumption are two of the most crucial problems of the contemporary world. The search for reliable, long-lasting sources of energy has been an ever-challenging task to the mankind. In this quest solar energy can be a reliable energy source. World's energy need is certain to increase with growth in population. We currently use 4.1×10^{20} J of energy per year, which is equivalent to ≈13 TW of power. This consumption may more than double to 30 TW by the year 2050 and then triple ≈46 TW by the end of the century (Sahaym and Norton 2008). The reserves of fossil fuels are just not sufficient to meet this requirement.

In the expedition for new energy sources, hydrogen is gaining attention as the most promising energy carrier. However, in order to implement the hydrogen economy, and completely replace fossil fuels by hydrogen, there are significant technical challenges that need to be overcome in each of the following areas: production and generation, storage, and conversion to electrical energy and heat at the point of use (Lin et al 2011). The intimate connection between hydrogen and electricity through fuel cells makes hydrogen much more relevant than just a clean substitute for fossil fuels. Hydrogen is an efficient energy carrier that has one of the highest energy density per mass of 140 MJ/kg. Hydrogen can combine with oxygen in a fuel cell to produce electricity

and water without generating pollutants, which makes it an environmentally benign fuel for the future. It is the stuff of stars and, when properly harnessed and produced from renewable sources, it is regarded as the "forever fuel" (Gonzalez et al 2011).

There is still a large gap between our present global energy consumption (around 13 TW) and the use of solar energy to supply the world's energy demand (being less than 2 %), and the enormous untapped potential of the sun (120'000 TW). Abundance of water on Earth makes it possible to break it into a clean and storable fuel (H_2) using sunlight (Currao 2007). Of the many approaches to produce hydrogen from renewable sources (especially solar energy) semiconductor-based photoelectrochemical (PEC) and photocatalytic (PC) splitting of water need specially mention. PEC splitting of water is a process whereby the light, illuminating a light absorbing photoelectrode (semiconductor) in an electrochemical cell, is used to split water into hydrogen and oxygen. This one-step more efficient system eliminates the need to first generate electricity from solar energy and subsequently feed it into an electrolyzer (Liu et al 2010). In its simplest form, a photoelectrochemical (PEC) hydrogen production device, consists of a semiconductor working electrode coupled with a counter electrode (usually platinum) dipped in an aqueous solution of electrolyte (Gupta et al 2009).

In the photoelectrochemical (PEC) water splitting following processes take place on irradiation of semiconductor electrode: photo generation of charge carriers (electron and hole pairs), charge separation and migration of the holes to the interface between the semiconductor and the electrolyte and of electrons to the counter electrode through the external circuit, and electrode processes that involve oxygen evolution through oxidation of water at the photo anode and release of H_2 through reduction of water at the cathode (Fujishima and Honda 1972).The photoelectrochemical (PEC) path to water splitting, thus, involves separating the oxidation and reduction processes into half-cell reactions. Exposure of semiconductor photoanode (usually n-type semiconductor) to sunlight results in charge transport within the PEC cell and evolution of gases at the photoanode and cathode. The oxygen energy level (O_2/H_2O) should be above the valence band of the photoanode in order to allow electron transfer and, for the same reason, the hydrogen energy level (H^+/H_2) should be below the Fermi level of the metal cathode (or the conduction band of a semiconducting photocathode). The most critical issue in the development

of solar hydrogen producing PEC device is the development of new and more efficient photosensitive materials for clean conversion of solar energy (Sharma et al 2011). A semiconductor, used as photoelectrode in PEC cell, must also be chemically as well as electrochemically stable with an optimum bandgap (≈ 1.8 eV) enabling it to absorb visible part of solar radiations. Semiconductors viz. TiO_2, $SrTiO_3$, SnO_2 and $BaTiO_3$, investigated as alternative photoelectrodes are of relatively high bandgap and cannot absorb large portion of visible light. On the other hand, low bandgap materials viz. Si, GaAs and InP get easily corroded in contact with the electrolyte (Jiang et al 2012).

Photocatalysis provides another useful method for storing the Sun's energy in chemical bonds that can be released later without producing harmful byproducts. The method has several advantages over direct solar-to-electric conversion. Traditional photocatalysts are able to efficiently convert solar to chemical energy under ultraviolet illumination, but not under visible illumination. Photocatalytic (PC) water-splitting provides a significant approach for clean, low-cost and environmental friendly production of H_2 by solar energy. However, in order to harness sunlight to produce hydrogen from water, there are three fundamental requirements that must be satisfied. Firstly, sunlight must be efficiently absorbed to generate electron/hole pairs for water-splitting. Secondly, either the recombination of the photo-generated electron/hole pairs or the backward reaction (recombination of H_2 and O_2 into water) must be prevented. Thirdly, undesirable reactions or products, such as photocorrosion or degradation of the photocatalyst must be prohibited (Yang et al 2009). Use of solar energy for photocatalytic water splitting using could contribute to the solution of environmental and energy issues related to the hydrogen production. Key research area in this field is the development of photocatalyst with high energy conversion efficiency. Semiconductor in form of metal oxide such as TiO_2, $SrTiO_3$, ZrO_2, Ta_2O_5, WO_3, and many others, were used as photocatalysts for water splitting to produce hydrogen (Dholam et al 2009). Materials with appropriate bandgap and adequate stability for water splitting under visible light irradiation are still unavailable and their development is considered a major challenge in photocatalysis research (Yue et al 2011). There are several issues that still limit the H_2 production rate on pure semiconductors. To solve these problems, many approaches have been proposed to enhance the photocatalytic activity of semiconductors, including the preparation of quantum-sized nanoparticles, deposition of noble metals, preparation of

heterogeneous semiconductors, and layered/Core shell structures. Recently, researchers have been focusing on the development of visible-light-responsive photocatalysts, because the ultraviolet (UV) light only accounts for about 4% of the solar radiation energy, while the visible light contributes to about 43% (Li et al 2011).

2. Metal oxide semiconductors for photo splitting of water

Photoelectrochemical (PEC) and photocatalytic (PC) splitting of water are promising approaches for hydrogen generation by harnessing solar energy. On this regard the synthesis and characterization of new and novel functional materials is of the utmost importance. Metal oxides semiconductors constitute an important class of materials that have been widely investigated with lots of promise for this purpose. Besides, they offer intriguing alternatives to overcome some of the technical barriers by rationally engineering the electronic bandgap structure to enhance charge transfer and transport and thereby improved performance (Kronawitter et al 2011).

Recently, there is growing interest in nanostructures/nanoarchitectures of metal oxides for above applications. Nanocrystals, nanocoral, nanosheets, nanotubes, nanowires, nanodots and nanorods of metal oxides offer advantages over their bulk counterparts due to their large surface area, short lateral diffusion length and low reflectivity. Nevertheless, most of the metal oxides have large bandgap energies, leading to limited light absorption in the visible region of interest, which imposes a fundamental limitation on overall photo-to hydrogen efficiency (Kronawitter et. al. 2011). Depending upon the size of the energy gap, a semiconductor can absorb light from a specific portion of the solar spectrum. To some extent we can manipulate the bandgap as well as other electrochemical properties by changing the particle size of the semiconductors and employing nanotechnology as a tool. The prospective semiconductor for efficient solar energy converters should have optimized band gap so as to be able to utilize maximum solar energy. Further, it should also have sufficient chemical stability against photocorrosion.

3. Layered/core shell Nanostructures/Nanoarchitectures

Layered/core shell nanostructures/nanoarchitectures of semiconductors have shown improved performance for PEC/PC splitting of water in few recent studies (Su et al 2011). Hence, such systems hold high promise in the solar energy conversion to directly usable chemical energy. In fact two basic approaches to the subject are being investigated with interest. One is to mimic natural photosynthesis by using organo-metallic sensitizers. While another strategy is to use layered /Core shell nanostructures of different semiconductors laid one over another (preferably a combination of low and high band gap semiconductors). Such structures provide unique characteristics for electron transfer processes as well as much wider light absorption window. There is no surprise that some layered structures have shown considerably high PEC activity (Tiginyanu et al 2011).

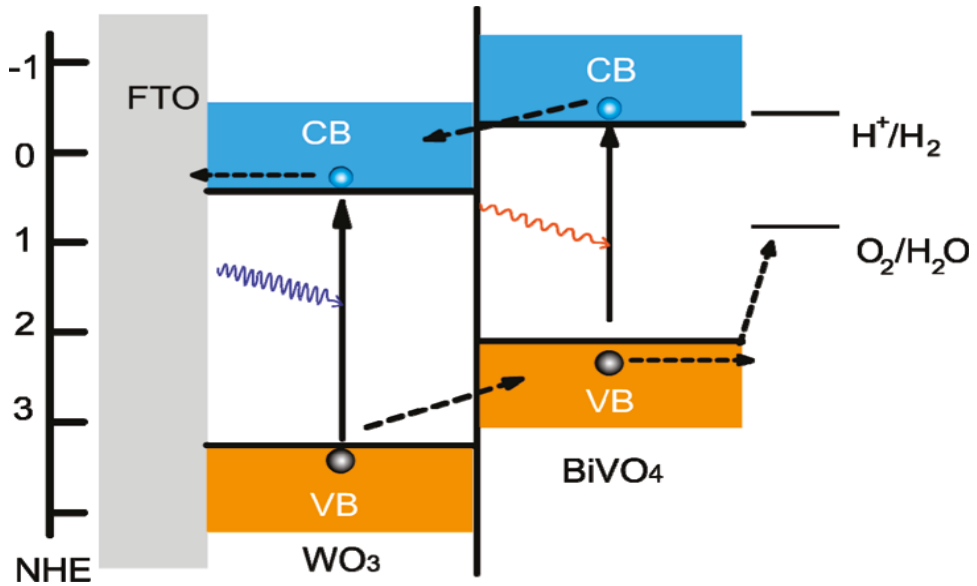

Figure 1: Energy diagram of the $WO_3/BiVO_4$ layered system (at pH 7) and electron transport processes therein (Reference: Su et al., 2011, *Nano Lett.*, **11**, 1928–1933).

The recombination of electrons and holes caused by low mobilities of holes and trapping of electrons are considered to be responsible for the low conductivities and poor photocurrent generation in PEC cells using metal oxide photoelectrode. According to this understanding photocurrent generation can be enhanced by increasing the conductivity or by improving the hole

diffusion length. (Logar et al 2012). The layered heterojunction electrodes are expected to reduce recombination of electrons and holes. When layered nanostructures are radiated with photon energy higher or equal to the band gap, the photogenerated electrons can move to the CB of low band gap semiconductor and the photogenerated holes to the VB of high band gap semiconductor. As a result, the formation of layered heterojunction may limit the charge recombination and improve the photo conversion of solar energy to hydrogen energy.

Layered nanocrystals have been the focus of scientific research almost since the beginning of colloidal synthesis of nanocrystals. Many so-called "Core-shell" particles, consisting of a core and a shell of a different semiconducting material, are known today (Liu et al 2010). When a particular dimension of one or both components of such heterostructures falls below the exciton wavelength, then various properties especially the optical band gap, are strongly modulated. Thus, to control the properties of such systems, it is important to be able to control the desired crystallographic phases formed in each layer and the dimensions and shape of the particles and then to be able to place each component in intimate contact with a second component having distinct electronic properties exerting at the same time some control over the interfaces. To some extent, the layered heterostructures can be considered a model system for the study of the structurally more complex heterostructures (Crabtree and Dresselhaus 2008).

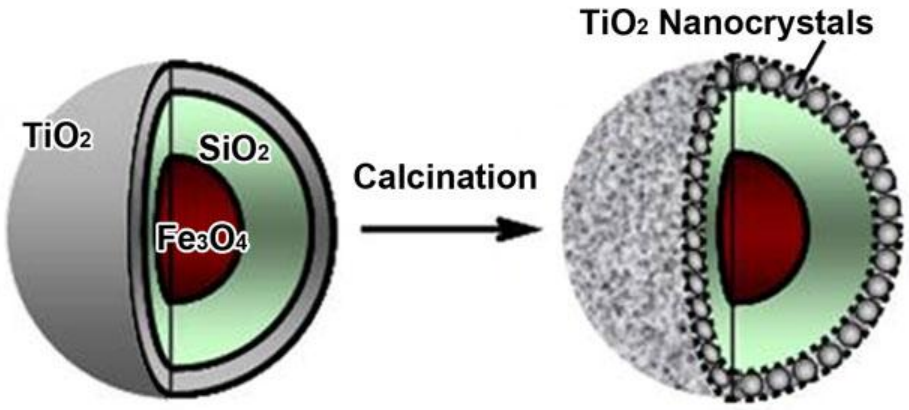

Figure 2: Core-shell Nanocomposites with Enhanced Photocatalytic Activity (Reference: Ye et al., 2010, *Chem. Eur. J.*, **16**, 6243-6250).

There are many semiconductor materials with small band gaps such as CdS, CdSe, PbS, MoS_2 and Cu_2O which absorb light in the visible region. Unfortunately, these materials exhibit photoanodic corrosion in the electrolyte and some are also toxic. The stability of these materials can be enhanced by including donors in the electrolyte, such as sulphite ions. This allows hydrogen production with minimized dissolution of the photoanode, but can suppress the oxygen production reaction. Thus, it is not a practical long-term solution. Materials with relatively wide band gaps such as TiO_2, ZnO, $SrTiO_3$, $KTaO_2$, ZrO_2 and SiC have good photo stability but exhibit limited light absorption and hence low efficiencies (Memar et al 2010). Layered/Core shell nanostructures represent an effort to couple the advantages of low and high band gap semiconductors, and at the same time limit their problem areas, in pursuit to an efficient PEC/PC device for solar hydrogen generation by photosplitting of water.

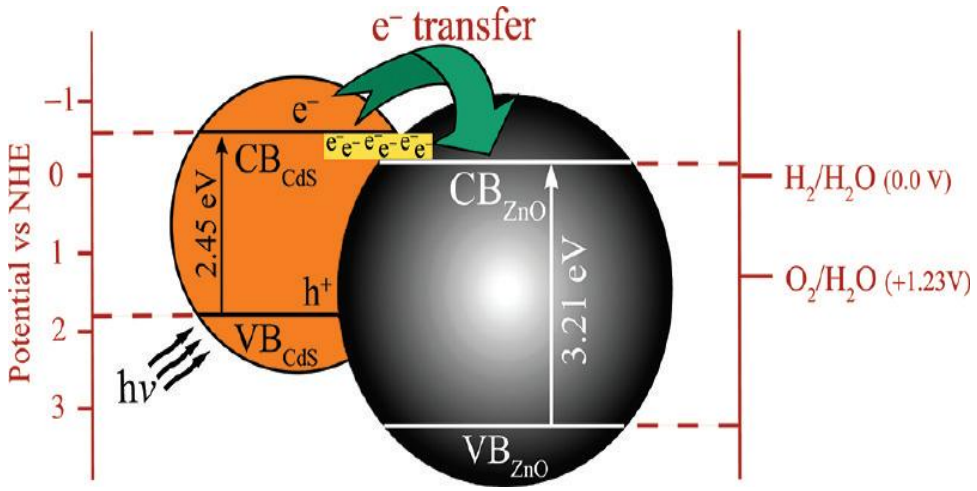

Figure 3: Schematic of band structures for CdS and ZnO layered structure and electron transfer therein (Reference: Barpuzary et al., 2012, *J. Phys. Chem. C*, **116**, 150–156).

4. Proposed Study

The genesis of the proposed work lies in the need to develop a greater insight on some of the above issues and the desire to build efficient PEC/PC systems for solar-hydrogen generation. The proposed study would be focused on the preparation and characterization of some layered/core shell nanostructures/nanoarchitectures of chosen metal oxides and investigates their performance in photo splitting of water. Materials of interest will be chemically stable oxides absorbing largely in the UV and visible region. The main thrust of the present study would be to explore the extent to which such nanostructures/nanoarchitectures of metal oxides get functionalized towards improved PEC/PC response for splitting water. The broad objectives/stages of the present study have been outlined below,

5. Objectives/Stages of the Proposed Work

The present study would essentially be based on photoelectrochemical and photocatalytic investigations using layered/core shell nanostructures/nanoarchitectures of chosen metal oxides for photosplitting of water. The study would have following broad objectives.

(a) The preparation of thin films of layered/core shell nanostructures/nanoarchitectures of metal oxides (thin film as well as powders) by wet chemical methods (sol-gel, precipitation, spray pyrolysis etc.).
(b) The physico-chemical characterization of samples prepared above for parameters mentioned in Table 1.
(c) Photoelectrochemical and photocatalytic investigations (pertaining to photo-splitting of water) using samples prepared under objective (a).

6. Proposed Methodology

Samples (films/powders) will be prepared by wet chemical routes using solution of metal salts as precursor. Films will be deposited on conducting glass substrate by spin-coating and/or dip-coating. Samples will be subjected to high temperature sintering to evolve the oxides crystalline phase. All the samples, thus prepared, will be characterized for structural, morphological, electrical/electronic and optical characteristics by standard methods using X-ray diffractometer, scanning electron microscope, atomic force microscope and UV-visible spectrometer The PEC studies will be performed by using prepared samples as working electrodes (WE) in the PEC cells by following the procedure described elsewhere (Sharma et al, 2011). Xenon Arc light source (150W, Oriel, USA) will be employed for illumination. PEC cells, filled with electrolyte, will be covered by a water jacket to prevent heating due to radiations. Electrolyte solution will be purged with N_2 for 5-15 min, before each PEC measurements. In PC studies samples will be used as photocatalyst in a reaction chamber where these will be dispersed in aqueous medium under irradiation and continuous stirring. The evolved hydrogen will be collected and analyzed.

7. Tentative Plan of the Work

A tentative plan of proposed work has been outlined below in Table 1

Table 1: Tentative plan of the proposed work

Parameters of the study	Description
Preparation of samples Materials of interest	Few of the following: ZnO, α-Fe_2O_3, CuO/Cu_2O, TiO_2
Proposed Avenues for Investigation	▪ Nanostructures/Nanoarchitectures ▪ Layered structures ▪ Core Shell structures
Proposed method for the preparation of samples	Wet chemical process (Sol-gel, precipitation, spray pyrolysis).

Expected variables in the study	**Preparation of samples:** ▪ Nature of metal oxides and their combinations ▪ Sintering Conditions: Temperature, Environment
Characterization	▪ Phase analysis by XRD ▪ Surface morphology by SEM ▪ Surface Topography by AFM ▪ Band gap energy by UV-Vis spectrophotometer ▪ Film thickness by surface profilometer ▪ Density ▪ Resistivity ▪ BET surface area measurement ▪ Flatband potential and carrier density
PEC measurement variables	▪ Current-Voltage characteristics of the PEC cell under darkness and illumination. ▪ Photovoltage & Photocurrent ▪ Open circuit potential ▪ Short Circuit current ▪ Onset voltage ▪ Applied bias photon to current conversion efficiency (ABPE)
PC measurement variables	▪ Qualitative and Quantitative estimation of hydrogen evolved ▪ Efficiency

(Shailja Sharma)

M.Sc. (Chemistry), M.Phil

Fujishima et al (1972) were first to report the photoelectrolysis of water using a single crystal of TiO_2 as the photoanode, at which oxygen was evolved. Electrons released from anode traveled by a wire to Pt electrode at which H_2 was evolved. The cell was chemically biased because the pH differed in cathodic and anodic compartments.

Fujihara et al (1977) reported that TiO_2, SnO_2, and $SrTiO_3$, do not undergo decomposition upon irradiation when used as photoelectrodes in aqueous media and are stable enough to be used for solar energy conversion and hydrogen production devices. The band gaps of these n-type semiconductors correspond to the energy of photons in the ultraviolet region. Solar energy reaching the earth's surface has, however, a spectrum distribution in the longer wavelength range and cannot, therefore, be used effectively by these semiconductors. Spectral sensitization may solve this problem by extending the sensitivity of the electrochemical photocells to longer wavelengths.

Drobny et al (1979) used reactive sputtering in oxygen- argon mixture to produce thin copper oxide films and its properties were easily controlled by varying the partial pressure of oxygen in the discharge. The properties of phase composition, resistivity and optical constants were investigated. The phase $Cu+Cu_2O$, Cu_2O, Cu_2O+CuO, CuO were identified and each phase exhibited characteristic values of resistivity and optical constants.Cu_2O prepared in that manner could be a useful thin film semiconductor material in view of its high refractive index in the visible range, its low value of extinction coefficient below 2.5 eV and readily controllable resistivity over the approximate range $25\text{-}10^4\Omega$ cm.

Redon et al (1981) investigated the photoelectrochemical properties of n-type semiconducting a flux-grown single crystal and a sputtered Fe_2O_3. Crystalline iron oxide showed n-type while sputtered iron oxide showed p-type behavior. The obtained band gap and flat band potential were 2.0 eV & 2.2 eV and +0.6 V & - 0.7 V (under illumination) for amorphous and single crystal compound, respectively. V_{fb} & band gap of iron oxide made by different methods and under different electrolytes were also determined.

Debnath et al (1982) assigned the three optical absorption peaks for hematite at 2.4, 3.2 and 5.8 eV to d → d and O 2p → Fe 3d charge transfer excitation. As expected, d-d absorption weak but may be expected to occur because octahedral symmetry is broken. The ellipsometric e_2 peaks at 2.2 and 3.0 eV matched the lower two transitions and also showed that d → d transition are weak. They assigned an absorption at 17 eV to O 2p → Fe 4s and O 2s → Fe 3d charge transfer excitations and explained the broadness in optical spectra of magnetite in terms of tetrahedrally split Fe^{3+} and octahedrally split d sets, the later due to average oxidation state of iron being 2.5.

Shinar et al (1982) carried out a photoelectrochemical study on the doped Fe_2O_3 with Si, Zr, Ti, Ta, W, Nb and V. A significant photocurrent was observed at zero value vs SCE in all the cases except TiO_2 doped electrode. Low resistance (10-20 Ω) was observed on sintering in the environment. The photocurrent measured at 400 nm were lower than those observed with the chemically doped electrodes, probably due to enhanced recombination of electrons and holes at the Fe_3O_4 produced at the electrode surfaces following the above treatment. Titanium doping was found to be less effective as compared to other + 4 ions and these electrodes were found to be stable.

Fujinaka (1983) studied thin films of cuprous oxide deposited on glass coated with transparent conducting indium-tin oxide (ITO) films. The deposition of both Cu_2O and ITO was made by r. f. sputtering in an Ar/O_2 gas mixture. The use of higher levels of O_2 flow resulted in an increased conductivity because of ad mixture of CuO to Cu_2O. The activation energy of 0.55 eV and band gap of 2.0 eV for Cu_2O was found from the spectral dependence of the photovoltaic effect. The Cu_2O film showed the typical XRD pattern of amorphous material.

Itoh et al (1984) prepared thin film electrodes of iron oxide by spray pyrolysis and studied the photoelectrochemical behavior of iron oxide films of different thickness in unmodified & modified electrolytic

solution. It was found that photoresponse was low for less thick film and increased on increasing the film thickness. High photocurrent was recorded in H_2O_2 added electrolytic solution as H_2O_2 acts as a strong reducing agent, *i.e.,* a hole scavenger, at the illuminated photoanode due to the less positive potential (0.86V *vs.* NHE).

Tafalla et al (1989) analysed the photocurrent transient behavior associated with flatband potential shifts during water splitting at n-TiO_2, electrodes. The effect of local pH changes and surface hole accumulation on the photocurrent transients observed during water photoelectrolysis at TiO_2, electrodes. With the help of the rotating disk electrode technique, the ratio between the stationary and the intial photocurrent was studied as a function of the rotation rate, at both pH 10.5 and 12.

Muckopadhyay et al (1992) reported the galvanostatic (at 40-60°) deposition method of semiconducting cuprous oxide thin films; important for low cost solar cell and oxygen or humidity sensor applications. XRD data revealed no other phases of copper oxide other than Cu_2O. The I-V characteristics of the Cu_2O films on copper exhibited MIS tunnel diode like characteristics. At room temperature resistivity of the film was found to be 2.6 x $10^3\Omega$ cm.

Ono et al (1992) investigated photoelectrochemical properties of iron oxide prepared by three different techniques (oxidative electrolytic iron plate, RF sputtered & sintered RF sputtered iron oxide). The maximum quantum yield was recorded for oxidative electrolytic plate of iron oxide for which threshold potential (Vp) for the onset of current under illumination was – 0.4V.

Badawy et al (1997) synthesized indium-incorporated TiO_2 thin films for solar cell fabrication by spray pyrolysis. The prepared n-Si/TiO_2-In solar cells exhibited better fill factor and solar conversion efficiency than those with pure TiO_2.The electrochemical properties of the prepared oxide films revealed that the charge transfer step at the oxide/electrolyte interface leads to the deterioration in quality of the photoanode.

Oscar et al (1998) achieved direct water electrolysis with a novel, integrated, monolithic potoelectrochemical-photovoltaic design. This photoelectrochemical cell, which is voltage biased with an integrated photovoltaic device, splits water directly upon illumination; light is the only energy input. The hydrogen production efficiency of this system, based on the short-circuit current and the lower heating value of hydrogen, is 12.4 percent.

Jayewardena et al (1998) studied the fabrication of n-Cu_2O electrodes with higher energy conversion efficiency in a photoelectrochemical cell. Photo response in cuprous oxide films, which were prepared by a simple method of immersing copper plates in a HCl solution of 3 pH at 40^oC temperature, when they were used in a PEC cell. This photoresponse was much higher than the previously published values for n-Cu_2O electrodes which were prepared by other methods. The photocurrent obtained was in the order of 0.3 mA/cm^2.when the cell was illuminated with light intensity of 50 mW/cm^2. (The semiconductor electrode was biased to get a zero dark current.) The power conversion efficiency of the cell was 0.01%. The maximum quantum efficiency obtained was 15%. It is hoped that these values could be improved with a better understanding of the photoelectrochemical properties of the cell.

Kudo et al (1999) fabricated all oxide-based, transparent polycrystalline p–n heterojunctions on a glass substrate. The structure of the diode was n+ ZnO electrode/n-ZnO/p-$SrCu_2O_2$ /In2-xSnxO_3 electrode on the substrate. They found that contact between the n- and p-type semiconducting oxides was rectified. The ratio of forward current to the reverse current exceeded 80 within the range of applied voltages of 21.5 to 11.5 V and the estimated diode factor (n value) was 1.62. The diode structure was fabricated on a glass plate with the total thickness of 1.3 μm and possessed an optical transmission of 70%-80% in the visible region.

Jongh et al (1999) prepared Cu_2O films galvanostatically at 55^0C and pH 11 at a current density of 0.2 mA cm^{-2}. XRD pattern showed the peaks corresponding to Cu_2O. The band gap was found 1.9 eV from optical measurements. SEM showed well defined crystals. Better cathodic photocurrent was observed with an air saturated solution (0.5 M Na_2SO_4 electrolyte) than by purging the solution with argon. In the presence of oxygen or methylviologen cation very efficient photocathodic reactions were found.

Yoon et al (2000) investigated the photoelectrochemical properties of the copper oxide thin film coated on the n-type silicon electrode as a function of film deposition temperature. XRD pattern of the film deposited at 200°C indicated the crystalline character of the CuO phase. When the copper oxide layer was thinner than 500 A°, the electrode showed a notable decay of the photocurrent. The highest photocurrent density and quantum efficiency were obtained for the n-Si electrode covered with a 700A° copper oxide thin film deposited at 200°C.

Ohta (2000) discovered that simultaneous H_2 and O_2 evolution can be achieved by just stirring the powder of a p-type semiconductor such as Cu_2O, NiO, Co_3O_4, Fe_3O_4 in distilled water at room temperatures. Frictional rubbing of the stirring rod onto the bottom of the glass vessel was an important condition. The friction between the stirring rod and the glass surface generates enough electrostatic fields to make a field emission of the positive holes from the semiconductor-powder which are fixed at the micro crack spaces on the glass surface. The emitted positive holes react with water molecules to evolve O_2 and protons, which go to the glass surface and combine with the electrons there to evolve H_2. The energy conversion mechanism, the generation of frictional electricity, the e.ect of water, the carrier tunneling emission probability, the hopping conduction in semiconductor, the effects of fluid dynamics, etc. were discussed.

Zaban et al (2000) prepared TiO_2 colloids by using hydrothermal method based on hydrolysis and pressure treatment of titanium isopropoxide precursor in acidic solutions. They studied the influence of the use of nitric and acetic acids during the synthesis and found a significant effect on the colloid crystal structure. Both dark-field TEM and phase transformation temperature measurements indicated that in colloids prepared in nitric acid, the surface structure difference affects the performance of dye-sensitized solar cells.

Ishizuka et al (2001) studied the effect of nitrogen doping into Cu_2O thin films by reactive radio frequency magnetron sputtering. The nitrogen was found to increase the hole density and act as acceptor but no defects were induced by nitrogen doping. The carrier density for specimen deposited at 400^0C was higher than that of 500^0C due to high rate of desorption of nitrogen from Cu_2O surface. There was no significant degradation of structural and optical properties by nitrogen doping. The Cu_2O thin film resistivity obtained was of the order of 15.2 Ωcm. The acceptor level for undoped and nitrogen doped Cu_2O were 0.25 eV and 0.14 eV respectively.

Jyoko et al (2001) prepared magnetic metal nanostructures by electrodeposition. Multilayered fcc Co/Pt nanostructures grown on a Pt (111) single-crystal substrate by electrodeposition under potential control exhibit a remanent perpendicular magnetization and a large magnetic coercivity, which depend on the multilayer growth mechanism. A possible interfacial alloying below the Pt overlayers induces a magnetic moment on the Pt atoms, leading to asymmetry between Pt/Co and Co/Pt interfaces of the multilayers. The role of the codeposition of Ni as an inhibitor for the nucleus growth process as well as for the dissolution of Co during the Pt deposition is of great importance for the occurrence of the multilayered nanostructure.

Balamurugan et al (2001) synthesized nanocrystalline Cu_2O thin films using activated reactive evaporation technique (at 30-200°C). The nanocrystalline size in films varied by varying the deposition parameters. The study indicated that high substrate temperature was required for the growth of Cu_2O phase in polycrystalline thin films. The Cu_2O phase was observed to be more stable in nanoparticles grown by chemical methods below 25 nm.

Stuart (2001) has reported multiple band gap semiconductor/electrolyte processers to convert optical energy. Such processes can incorporate either a schottky or an ohmic Photoelectrochemical solution interface that can drive either regenerative single or multiple redox reactions Ga As/Si or Al Ga As/Si each have a solar to electrical conversion efficiency of 19-20%. A cell containing illuminated AlGaAs/Si RuO_2/Pt black evolves H_2 and O_2 at record (18%) efficiency, further multiple band gap/electrolyte systems are calculated as being capable of attaining over 30% solar efficiency.

Balamurugan et al (2002) deposited nanocrystalline copper oxide thin films by activated reactive evaporation and studied the effect of 120 MeV $107Ag^{9+}$ ion irradiation on structure, size and surface. They observed the transformation of CuO phase to Cu_2O during ion irradiation (5×10^{12} and 10^{13} ions cm^{-2}). The average crystallite size was also increased on irradiation from 4.9 nm to 6 nm as calculated by Scherrer's equation. The bandgap was found to decrease from 2.48 to 2.39 eV, upon irradiation.

Nakaoka et al (2002) deposited p-type cupric oxide electrochemically on platinum and gold electrodes from Cu (II) solutions containing various amino acids. Current-potential curves for a CuO deposited electrode under the irradiation of light and dark showed that the onset of the photocurrent was at about -0.05V (vs. Ag/AgCl), giving a positive potential shift of about 0.2V from the dark current rise. Hence, the CuO electrode was found to exhibit a p-type semiconductor behavior. The grain size of the deposited CuO estimated from the from the diffraction peak of (110) depended on the amino acid used such as, 12(Gly), 32(Ala), 30 (Ile).

Borgohain et al (2002) synthesized Cu_2O nanocrystals using two different synthesis techniques: (a) conventional chemical route and (b) a novel electrochemical method. The chemical route involved heating of copper tartarate complex with glucose in the presence of a capping agent polyvinyl pyrrolidone (PVP). Average particle diameter from TEM for Cu_2O-II and Cu_2O-III nanocrystals were 5.0 and 10.0 nm, respectively. Selected Area Electron Diffraction (SAD) patterns of the crystals showed concentric rings corresponding to (111), (200), (220), (311), (331), and (420) lattice planes of cubic Cu_2O. Electron pattern also showed formation of single-phase Cu_2O nanocrystals and no CuO formation was detected.

Shukla (2002) have reported the formation of polycrystalline TiO_2 3lm (rutile phase; tetragonal: a=4:593 8A and c=2:959 A8) by anodic oxidation of titanium sheet. The microstructural characterization revealed the porous nature of the 3lm consisting of randomly oriented microcrystals. The hotoelectrochemical (PEC) characterization of TiO_2 films has been carried out by employing standard electrochemical techniques. The hydrogen production rates were found to be 37.4 and 24:6 l h^{-1} m^{-2}, respectively, for PV biased PEC and PV (stand-alone) driven electrolysis modes.

Miller et al (2003) designed considerations for a hybrid amorphous silicon/photoelectrochemical multijunction cell for hydrogen production. Triple-junction amorphous silicon (a-Si) solar cells demonstrating photovoltaic (PV) efficiencies up to 12.7% and open-circuit voltages up to 2:3 V The fundamental design strategy for producing such high efficiency in multijunction amorphous silicon devices involved careful current matching in each of the junctions by adjustment of the absorption spectra through bandgap tailoring. Typically, the top nip junction in a-Si triple-junction cell is designed to absorb most strongly in the 350 –500 nm range.

Feng et al (2003) studied the photocatalytic properties of bismuth titanate ($Bi_{12}TiO_2O$) crystals. They prepared ($Bi_{12}TiO_2O$) crystals by chemical decomposition method and the band gap of $Bi_{12}TiO_2O$ crystals was estimated to be about 2.4eV from UV-Vis absorption spectra of the photocatalyst. They studied photo-decolourization of methyl orange using $Bi_{12}TiO_2O$ solution.

Bassehouad et al (2003) prepared $CuMnO_2$ by solid state reaction from stoichiometric amounts of binary oxides and sintering in a tube at 960°C. I-V characteristics were measured using 1M KOH (pH- 13.4) using 500W halogen lamp. They observed that the $CuMnO_2$ synthesized at lower temperature (590°C) has higher specific surface and improves the hydrogen production by about 30%. They used it for H_2S degradation in which hydrogen was produced additionally.

Zhou et al (2003) demonstrated different morphologies of oxide nanostructures under different oxidation temperatures. The study indicates that oxide morphology is controlled by kinetics and thermodynamic factors during oxidation process. The study led to Cu_2O island formation as a function of oxidation temperature in the range of 150-1000°C. The size of Cu_2O island increased with continued exposure to oxygen but there was no change in the shape of the island shape. Both in situ TEM & AFM investigation revealed the edges of all the square shape islands formed at higher temperatures have roughly equal growth rates along these four equivalent crystallographic orientations which results in the four folded symmetry of island.

Getoff et al (2003) prepared multilayer semiconductor electrodes based on silicon for H_2 production. In their work to obtain semiconductor anodes with a high photosensitivity and with long-term corrosion resistivity, Si wafers were coated with a thin layer of Ni or Co. The cleaning, coating and the thermal annealing procedures of the samples are of crucial importance. During the operation of the electrodes in the cell, very stable multilayer photoanodes are formed. The data obtained by studying the photocurrent density (mA cm^{-2}) as a function of applied voltage, action spectra, etc., show that both Ni and Co are rather appropriate as protecting materials, leading to photoanodes with good corrosion resistance and photoefficiency.

Riess et al (2004) studied solid state devices based on Cu_2O for current voltage relationships by assuming schottky barriers to exit between a metal electrode and the oxide. The symmetric nature with respect to origin indicated the uniform distribution of oxygen interstitials in the oxide layer. Under fast measurements the accepters are frozen and also due to oxide acting as semiconductor with a fixed, homogenous or non homogenous, distribution of acceptors and holes yielding only a linear I-V relation.

Bernal et al (2004) reported the preparation and properties of Co-Fe mixed oxides obtained by calcination of layered double Hydroxides. They have been characterized by powder X-ray diffraction, FT-IR spectroscopy, thermal analysis (differential thermal analysis, thermogravimetric analysis and temperature-programmed reduction. Thermal decomposition takes place in a single step up to ca. 350°C, and the specific surface area increases with the iron content, probably because of the presence of hydrated amorphous iron oxides. The solids calcined at 1200°C in air contain crystalline CoO, Co_3O_4 and $CoFe_2O_4$ (spinel), this one being the dominant phase, and only phase detected for large Fe contents. Metallic species are more easily reduced in the original solids than in the calcined ones, and in all cases iron seems to be reduced at a higher temperature than cobalt.

Aroutiounian et al (2005) presented results in the field of photoelectrochemical splitting of water. Determining the efficiency of Photoelectrolysis and possible ways to increase the photocatalytic activity of semiconductor photoelectrodes are analyzed. It is shown that the development of new photoelectrodes made of solid solutions and more complicated multicomponent compositions are most promising.

Ingler et al (2005) studied the Photoresponse of spray pyrolytically synthesized magnesium-doped iron (III) oxide (p-Fe_2O_3) thin films under solar simulated light illumination. Stable Mg-doped iron (III) oxide thin film electrodes that exhibit p-type behavior were synthesized by spray pyrolytic methods on indium doped tin oxide-coated glass substrate. The highest photocurrent density of 0.22 mA/cm^2 was observed for Mg-doped p-Fe_2O_3 samples. The total spray time for optimized photoconversion efficiency of 0.33% was found to be at 130 s for a spray period of 10 s. X-Ray diffraction (XRD) studies revealed mixed structures (a and g-Fe_2O_3 and MgO) for the Mg-doped p-Fe_2O_3 thin films

Liu et al (2005) reported the preparation and characterization of cerium oxide doped TiO_2 nanoparticles. The Ce doped TiO_2 powders could apparently shift the UV-absorption band of TiO_2 toward visible range, and there was an optimal Ce content in association with the maximum absorbance. According to X-ray photoelectron spectroscopy (XPS) investigation, the Ti element mainly existed as the chemical state of Ti 4C and the Ce oxide doping did not affect the peak position of Ti 2p. The Ce 3d spectrum of Ce doped TiO_2 sample basically denotes a mixture of Ce 3C/4C oxidation states giving rise to a myriad of peaks.

Kitiyanan et al (2005) studied the preparation and characterization of nanostructured TiO_2 ZrO_2 mixed oxide electrode for efficient dye-sensitized solar cells. The mixed zirconia (ZrO_2) and titania (TiO_2) mesoporous powder possessed larger surface area than the corresponding titania. For the UV action spectra of unsensitized photochemical cell, the mixed zirconia/titania electrode can absorb UV light below 380 nm, corresponding to band gap (E) around 3.27 eV, which is higher than that of pure component of titania (E ¼ 3 :2 eV). Solar energy conversion efficiency was up to 17%.

Jeong et al (2005) prepared silver-doped ZnO (SZO) films by rf magnetron sputtering on glass substrates. The SZO films have a preferred orientation in the (002) direction. As amounts of the Ag dopant in the target were increased, the crystallinity as well as the transmittance and optical band gap were decreased while those properties were degenerated at 200°C. And as the substrate temperature was increased, the crystallinity and the transmittance were increased. Changes of optical band gap for the SZO films were explained with the data obtained by XRD, XPS and using near-edge X-ray absorption fine structure (NEXAFS) spectroscopy

Miyake et al (2005) prepared Fe_2O_3-Nb_2O_5 coating films of various Nb/ (Fe + Nb) mole ratios by sol-gel method. On increasing the Nb/ (Fe + Nb) molar ratio from 0 to 0.25, the crystalline phases changed from α-Fe_2O_3 to α-Fe_2O_3 + $FeNbO_4$ and the photoanodic current under monochromatized light illumination increased both in the visible and UV ranges. The photoresponse extended to 600 nm, and IPCE was the maximum (18%) at the wavelength of 325 nm for the sample consisting of R-Fe_2O_3 and $FeNbO_4$ (Nb/ (Fe + Nb) = 0.25).

Liu et al (2006) studied the electronic structure and visible light catalysis water splitting property of Cr doped strontium titanate synthesized by low temperature solvothermal reaction. The absorption patterns of $SrTi_{1-x}Cr_xO_3$ were highly dependent on the dopant concentration. On increasing the amount of chromium, the number of absorbed photons increased which in turn gave better photoresponse.

Murphy et al (2006) compared the measurements of efficiency performed under xenon lamp and solar illumination were compared with efficiencies calculated by integrating the incident photon conversion efficiency (IPCE) over the lamp and solar spectra. It was observed that use of a xenon lamp as the light source could lead to a large overestimate of the photoconversion efficiency, relative to that obtained under standard AM 1.5 solar illuminations. The overestimate was greater when a water filter is fitted to the xenon lamp, and when a wide-band gap semiconductor, TiO_2 was used as the photoelectrode.

Mishra et al (2006) had done the study of modular PEC solar cells for photoelectrochemical splitting of water employing nanostructured TiO_2 photoelectrodes. For fabrication of cell, photoelectrodes in the form of nanostructured TiO_2 film over Ti-metal base have been synthesized by alkoxide sol–gel method using Ti $[OCH(CH_3)_2]_4$ as precursor followed by deposition using spin on technique. Crystalline phase and microstructure of the deposited film have investigated with the help of X-ray diffraction and TEM techniques. The rates of hydrogen production have been determined by measuring volume of the gas evolved over cathode, which is corresponds to ± 0.40 cm^2.

Huaming et al (2006) prepared sphere shaped and well dispersed nanoparticles with average crystal size of 35 nm of cubic Cu_2O via the electrochemical method. Photocatalytic degradation of methyl orange (MeO) in Cu_2O solution was primarily investigated to evaluate the photocatalysed efficiency of the as-prepared Cu_2O. Ninety-seven percent of MeO was decolorized with 2 g/L of Cu_2O catalyst under UV irradiation for 2 h and under sunlight for 3 h.

Prakasam et al (2006**)** synthesized self-organized nonporous iron (III) oxide (haematite) via potentiostatic anodization of iron foil. By varying the applied potential and electrolytic composition, the pore diameters range from 50 to 250 nm with a pore depth of 500 nm. The effect of electrolytic composition, anodization bath temperature and applied potential on the dimensions of the as-synthesized nanoporous structure was also examined. The photolelectrochemical studies were made in presence of highly oxidisable specie, H_2O_2. The crystallized nanoporous film, having a 2.2 eV bandgap, exhibited a net photocurrent density of 0.51 mA cm^{-2} in 0.5 M H_2O_2 +1 M NaOH at 0.6 V versus Ag/AgCl under simulated AM 15 sunlight. The introduction of H_2O_2 in electrolyte increased the photocurrent and lowered the onset potential.

Wijesundera et al (2006) investigated the potentiostatic electrodeposition of single phase Cu_2O and Cu thin films on Ti substrates in a potential range of 0 to -300 mV Vs SCE and -700 to -900 mV Vs SCE respectively. Cu_2O thin films with cubic shaped grains of the order of ~ 1 to 2 µm can be possible at the deposition potential around -200mV Vs SCE. Dark and light current voltage measurements in a PEC cell revealed that the photoactivity of the Cu_2O thin in a PEC can be improved by depositing microscopic scale random Cu deposits on the top of Cu_2O thin films.

Kelly et al (2006) designed a robust photoelectrochemical device to generate hydrogen using solar water splitting. Solar water splitting using photoelectrochemical (PEC) devices based on triple-junction amorphous silicon (a-Si) solar cells has the potential to offer an inexpensive, efficient, and renewable source of hydrogen for the future hydrogen economy. Triple-junction a-Si cells coated with indium-tin oxide (ITO) and arranged so that the outer semiconductor layer was "p-layer" split water in alkaline electrolytes. However, such PEC devices only operated for a few hours and with solar to hydrogen efficiencies of less than 3%.

Garuthara et al (2006) electrodeposited thin films of Cu_2O on ITO substrates for photoluminescence characterization. Photoresponse of the film clearly indicated the films to exhibit n-type behavior of Cu_2O in phototelectrochemical cells. The analysis of PL spectra as a function of temperature and excitation laser intensity allowed identifying the intrinsic defects in n-type Cu_2O. The film consisted of O2 vacancies which create a donor energy level of 0.38 eV below the bottom of the conduction band. This work indicates that oxygen vacancies create n-type conductivity in Cu_2O.

Mathew et al (2006) discussed the effect of doping spray pyrolyzed thin films of In_2S_3 with silver. It was observed that silver diffused into In_2S_3 films in as deposited condition itself. Depth profile using x-ray photoelectron spectroscopy clearly showed diffusion of silver into In_2S_3 layer without any annealing. Band gap decreased up to the optimum value of doping and thereafter it increased. Electrical studies showed a drastic decrease in resistivity from $1.2X10^3$ to 0.06 Ω cm due to doping. A sample having optimum doping was found to be more photosensitive and low resistive when compared with a pristine sample. Improvement in crystallinity, conductivity, and photosensitivity due to doping of spray pyrolyzed In_2S_3 films with Ag helped to attain efficiency of 9.5% for Ag/ In_2S_3 /$CuInS_2$ /ITO indium tin oxide solar cell.

Changdong et al (2007) prepared electrochemically ZnO thin films deposited onto the ITO coated glass substrate from an electrolyte consisted of 0.1 M $Zn(NO_3)_2$ aqueous solution at 65 - 108ºC. The as deposited ZnO thin films were transparent to visible light and the average optical transmittance values of films were high to about 80–90%. The band gap energy of about 3.5 eV for the as-deposited ZnO films was independent of the applied potential and the deposition time. It was indicated from the FT-IR measurements that the minor amount of $Zn(OH)_2$ might be co-deposited with the formation of ZnO, which was contributed to the high Eg of the as-deposited films. The PL spectra of the ZnO films indicated that the decrease of the applied potential, increase of the deposition time at a certain potential, and annealing process after as-deposition would improve the crystalline quality of the as-deposited ZnO films.

Evic et al (2007) prepared amorphous SiO/SiO_2 superlattices by high-vacuum evaporation of 3 nm thin films of SiO and SiO_2 (10 layers each) onto Si (1 0 0) substrate and a study on amorphous SiO/SiO_2 superlattice performed by grazing-incidence small-angle X-ray scattering (GISAXS). The size of the growing nanoparticles in the direction perpendicular to the film surface is well controlled by the bilayer thickness. However, their size varies more significantly in the direction parallel to the film surface.

Haga et al (2007) studied the bottom-up approach to functional nanoscale architectures from molecular components. The self-assembly of an anchor monolayer on solid surface, layer-by-layer growth proceeded with the assistance of metal coordination, resulting in multilayer structures. The fixed arrangement of molecular units on surface affords a uniform response to external stimuli and a predetermined distance for electron transfer on the electrode surface, which provides novel molecular electronic devices.

Bjorn et al (2007) fabricated tungsten oxide films at low processing temperatures *(*< 250 ◦C) by reactive sputtering from tungsten targets in an argon/oxygen ambient. The films showed dense, compact morphology and columnar growth. A maximum photocurrent of 2.7mA/cm2 (at 1.6V vs SCE) was observed in 0.33M H_3PO_4 under AM 1.5 Global illuminations. Doping of sputtered tungsten oxide films with nitrogen resulted in a red-shifted absorption edge. The maximum photocurrent of a nitrogen-doped sample was measured at 2.3mA/cm2 (at 1.6V vs SCE). A multi-junction photoanode based on the best available sputtered WO_3 film and an amorphous silicon photovoltaic device was projected to operate at 2.2% solar-to-hydrogen efficiency.

Mohapatra et al (2007) designed PEC cell using carbon doped titanium dioxide nanotube arrays as the photoanode and platinum, Pt nanoparticles incorporated in TiO_2 (titania) nanotube arrays, as the cathode. The photoanode was prepared from highly ordered titania nanotube arrays by the sonoelectrochemical anodization method using ethylene glycol and ammonium fluoride solution. The cathode was prepared by synthesizing Pt nanoparticles on TiO_2 nanotube arrays by the incipient wetness method. The photocurrent density was found to be 2.5 – 2.8 mA/cm^2 at – 0.4 $V_{Ag/AgCl}$. The efficiency of the PEC cell using UV and visible light was found to be 13.3% and 8.5%, respectively.

Wenjun et al (2007) prepared the electrodes of WO_3, Fe_2O_3 and WO_3/Fe_2O_3 on a FTO substrate by a sol–gel method. The absorption of WO_3/Fe_2O_3 originated mainly from Fe_2O_3. The semiconductor electrodes generated anode photocurrent, which suggested they were n-type semiconductors. The IPCE of the heterojunction was much higher than that of WO_3 or Fe_2O_3 alone under light with different wavelengths, particularly in the visible region. The photo-generated electrons in the WO_3 were transferred more easily through the Fe_2O_3 layer in the heterojunction electrode. Effective separation of electrons and holes in WO_3/Fe_2O_3 was attributed to the photocurrent enhancement.

Aroutiounian et al (2007) synthesized ceramic semiconductor photoelectrodes made of Fe_2O_3 with up to 2 at% Sn-doping. The introduction of quadrivalent tin ions results in the transformation of Fe_2O_3 into an n-type semiconductor. Sn-doping level highly influenced the flat band potential of Fe_2O_3 electrode in 1M NaOH solutions. The photocurrent onset was approximately -0.25V for photoelectrode with 0.5 at% Sn, and photocurrent onset was shifted anodically with heavier dopings, becoming almost constant at ca. – 0.14V.

Chengkun et al (2007) synthesized Carbon modified (CM)-n-TiO_2 nanotube arrays by anodization of Ti metal sheet in fluoride solution and subsequent annealing in air and natural gas flame oxidation. Both nanotube structure and carbon doping contributed to the enhancement of photoresponse of n-TiO_2. About two fold increase in photocurrent density was observed at undoped n-TiO_2 nanotube film compared to that at its undoped n-TiO_2 flat thin film. Also, about eight fold increase in photocurrent density was observed at carbon modified (CM)-n-TiO_2 nanotube film compared to that at undoped n-TiO_2 flat thin film. The sample prepared by anodization at 20V cell voltage for 20 h followed by annealing in air at 500 1C for 1 h and natural gas flame oxidation at 820 1C for 18 min produced highest photocurrent density. It was found that the bandgap of n-TiO_2 was reduced to 2.84 eV and an additional intragap band was introduced in the gap at 1.30 eV above the valence band.

Kumari et al (2007) studied the photoelectrochemical behavior of Cd-doped titanium oxide thin film, prepared by sol–gel method, as a function of doping concentration and film thickness. Best photoresponse was recorded for doping with 1.0 at % Cd. Further increase or decrease in doping concentration led to fall in the photoresponse. The observed band gap energy decreased from 3.5 to 2.9 eV on increasing the dopant concentration from 0.5 to 2.0 at%. Flatband potential and donor density, determined from Mott–Schottky plots, were found to vary from −0.98 to −1.46 V/SCE and 5.7×1018 to 2.9×1019 cm−3, respectively.

Antonio (2007) presented a short review on semiconductor based photoelectrochemical water splitting into hydrogen and oxygen using sunlight as the energy input. To halt the buildup of carbon dioxide, the development of an alternative energy source to fossil fuel becomes more and more important.

Wenfeng (2007) in his paper overviewed the promotion effects of nanosized modifications in the interlayer and surface of photocatalysts for H_2 evolution. The Photocatalytic activity depends on modification technique as loading, proton exchange and intercalation. Cadmium sulfide intercalated composites showed higher activity and stability.

Wang et al (2007) deposited Copper (I) oxide (Cu_2O) films by electrochemical deposition method on Sn-doped indium oxide substrates. The influence of electrodeposition bath pH on grain orientation and crystallite shape was carefully re-examined using X-ray diffraction and scanning electron microscopy. In addition to the (100) & (111) preferred orientations identified in two previous sets of studies, as the bath pH was varied in the present study from 7.5 to12, a third preferred orientation, (110), was identified in narrow pH range, 9.4 to 9.9. A remarkable shift in the flatband potential was measured in a non-aqueous electrolyte medium for the various Cu2O samples obtained from baths of varying pH.

Guillen (2008) the prepared nanostructured ZnO electrodes prepared from ZnO nanoparticles and sensitised with xanthene dyes performance of Eosin Y, Eosin B and Mercurochrome was compared to the more common N719 dye. It was observed that these dyes efficiently sensitized ZnO nanopowder and yield efficiencies that were very competitive with respect to those provided by N719. Local photocurrent and transmittance measurements as a function of the wavelength confirmed the good performance of the xanthene dyes in the absorption maxima. They prepared polymer-sealed cells and measured the short-circuit current of the devices under continuous illumination at 200mW/cm^2 corresponding to twice the standard solar light intensity. The organic dyes showed very good stability properties under these conditions.

Che-Chia et al (2008) have prepared different p-type Cu_2O powders from electrodeposition and subjected to analysis of their photocatalytic activity in water reduction. Under illumination the Cu_2O powders alone were not able to catalyze H_2 generation. However, these exhibited Photocatalytic activity when coupled with n-type WO_3 in suspensions. Coupling was made to avoid back reaction.

Maria et al (2008) have carried out Photoelectrochemical decomposition of ethanol in a two-electrode chemically biased Photoelectrochemical cell by employing commercial nanocrystalline titania deposited on a conductive transparent electrode as photoanode. Hydrogen was generated in the Pt cathode compartment.

Eun (2008) a water-splitting reactor yielding hydrogen and oxygen was designed with a titanium oxide (TiO_2) nanotube array photoelectrode vertically grown on a titanium substrate. The TiO_2 nanotube arrays were made by the method of anodization and annealed in an oxygen atmosphere. Hydrogen gas was collected from the reactor and the exact amount of hydrogen gas evolved from the photoanode was analyzed. The relationship between the amount of hydrogen evolution and three key factors, viz. the tube length, tube structure and crystal structure, was investigated.

Sun et al (2008) synthesized carbon-doped In_2O_3 films by spray pyrolysis and valuated for photoelectrocatalysis. C-doped In_2O_3, compared to undoped, showed increased absorption in the 350–500 nm range with a red shift in the band gap transition. The photoactivity was evaluated under near-UV and visible light irradiation. The C-doped films exhibited photocurrent densities up to 1 mA/cm^2, with a high contribution (40%) from visible light irradiation. Under the same irradiation conditions, C-doped In_2O_3 produced much greater photocurrent densities than the undoped films. Under UV–visible light irradiation, the photocurrent densities of the C-doped In_2O_3 are at least five times higher than for the undoped In_2O_3 electrode at 0.7 V, and these were obtained without any sacrificial reagents.

Tomas et al (2008) developed terrylene chromophore exhibiting a high extinction coefficient as a sensitizer for photovoltaic applications. The photophysical and photochemical properties of the dye were analyzed. Terrylene-sensitized nanocrystalline TiO_2 solar cells yielded good photocurrents providing more than 60% in external quantum efficiency. The photoinduced electron transfer from the dye to TiO_2 was found to be very sensitive to conduction band edge shifts in TiO_2 induced, either by changes in the composition of the redox electrolyte or by UV illumination. This sensitivity was observed in quantum efficiencies for photocurrent generation of terrylene-sensitized solar cells and in photoinduced absorption experiments. The conduction band shifts were quantified using charge extraction methods. The observed sensitivity of the injection efficiency suggests that photoinduced electron transfer occurs from the relaxed excited state, possibly due to poor electronic coupling between TMIMA excited states and TiO_2 conduction band states.

Haijian et al (2008) prepared sulfur-doped TiO_2/Ti photoelectrodes. In which S^{4+} and S^{6+} were dispersed on the surface of TiO_2 nanoparticles. The doping with sulfur, expanded the response range of TiO_2/Ti photoelectrodes to visible light, and enhanced the separation of photoinduced electrons from cavities. The photoelectrocatalytic performance test run with sulfur-doped TiO2/Ti photoelectrodes under Xenon light indicated that Na_2SO_3 concentration of 750 mg/L and voltage of 160V were the optimal conditions for preparation of sulfur-doped TiO_2/Ti photoelectrodes.

Martıinez-Ruiz et al (2008) deposited Cu_2O and Cu nanoparticles on the surface of multi-walled carbon nanotubes with a diameter range of 15–90 nm by the impregnate method. Multi-wall carbon nanotubes with a length of 200 mm and a diameter range of 70–110 nm were grown inside of quartz tube by the spray pyrolysis method using ferrocene/benzene under argon flow. The cuprite and copper nanostructures were prepared in situ on the CNTs during thermal treatment at 300°C; the temperature at which the reaction occurred between the Cu and carboxylate functionalities of the nanotube surface. The average size of evenly distributed nanoparticles on the surface of MWCNTs had been in the range of 15–90 nm.

Wang et al (2008) prepared adherent, dense and transparent ZnO thin films on seeded glass substrate in aqueous/ethanolic solution via a simple CSD process. As-deposited films consisted of nanocrystals with their orientation being tuned by varying the volume ratio of water to ethanol. The film deposition rate decreased with increasing ethanol content in the solution, and the film thickness was increased by extending the deposition time at a given ethanol content. The CSD ZnO films exhibited intense UV emission with the LT and RT peaks being ascribed to bound excitons and free excitons, respectively.

Randeniya et al (2008) prepared S-doped TiO_2 for photoelectrochemical hydrogen generation from water by three different techniques (first two involved ball milling and third was sol-gel method). In all cases, the powder showed absorption in visible portion of the spectrum. Films of thickness around 0.5-0.8 μm offered best

photocurrent. All coating showed the presence of Nitrogen in the form of hyponitrite and nitrate ions and sulfur in the form of sulphate ions, except after very long heat treatment.

Dholam et al (2008) synthesized TiO_2 thin films by radiofrequency sputtering and sol-gel method to study the hydrogen generation by photocatalytic water splitting under visible light irradiation. The absorbance edge of TiO_2 film deposited by sputtering was at the higher wavelength as compared to the sol-gel derived film. It was observed that Voc decreases on increasing the ITO thickness while reverse was observed for sol-gel derived films. The H_2 production rate was measured to be 12.5 ± 0.1 and 4.3 ± 0.1 μmol/h for the sputter and sol-gel deposition.

Arena et al (2008) synthesized multi-wall carbon nanotubes (MWCNTs) by catalytic chemical vapor deposition (CCVD) over Fe supported on alumina catalyst, using isobutane as feedstock and were dispersed in aqueous solutions of sodium dodecyl sulfate. Stable and highly photosensitive hetero junctions were developed by liquid-phase deposition of MWCNTs/surfactant mixtures on the top of n-doped monocrystalline silicon wafers. Electrical measurements performed in the dark & under illumination showed that the hybrid solar cells, despite their non-optimized design, have conversion energy efficiency of the order of 3%.

Tsay et al (2008) deposited Sn doped ZnO films onto alkali-free glass substrates by a sol–gel method. The as-deposited films were annealed in air at 500 °C for 1 h. It was observed that Sn doping in ZnO thin films markedly decreased the surface roughness, improved transparency in visible range, and gave a finer microstructure than that of undoped ZnO thin films. The energy bandgap of ZnO:Sn thin films was about 3.23–3.27 eV. The ZnO:Sn thin film with 2 at% Sn exhibited the smoothest surface morphology, the best average transparency of 90% and the highest resistivity of 9.3×102 Ω-cm.

Paulauskas et al (2008) investigated single crystals of various n-type semiconducting oxides for PEC splitting of water. Current density vs. applied potential measurements indicated that all of the crystals exhibited diodic properties when in contact with a highly basic electrolyte. It was observed that the spectral quantum yield of the crystals was related to the penetration depth of the incident light, meaning that electron–hole pairs formed far from the semiconductor–liquid junction were less likely to be collected than those formed near the surface. The quantum yield was found to decrease with time.

Radecka et al (2008) synthesized titanium dioxide photoanodes doped with chromium (up to 16 at%) and tin (up to 50 at%) by RF reactive sputtering. Electrochemical studies were made in a three-electrode PEC cell with a TiO_2 thin film photoanode immersed in liquid electrolyte Mott-Schottky plots and photocurrent.

Han et al (2008) have investigated the effects of an embedded silver layer on the electrical and optical properties of zinc oxide ZnO/silver Ag/zinc oxide ZnO layered composite structures on polymer substrates. Hall effect, four-point probe, and UV-Vis spectrophotometer analyses were used to characterize electrical and optical properties. The results showed that carrier concentration, mobility, and conductivity increase with Ag thickness. Increasing Ag thickness from 8 to 14 nm enhances sheet resistance and resistivity by six orders of magnitude. The optical transmittance of the composite structure decreases when compared to a single ZnO layer of comparable thickness.

Behnajady et al (2008) prepared silver doped TiO_2 nanoparticles by liquid impregnation (LI) and photodeposition (PD) methods and characterized them by scanning electron micrographs (SEM) and X-ray diffraction (XRD). The photocatalytic activity of silver doped TiO_2 was tested by photocatalytic degradation of C.I. Acid Red 88. Result showed that silver doped TiO_2 was more efficient than undoped TiO_2because of its ability to trap electrons. This process reduces the recombination of light generated electron-hole pairs at TiO_2 surface. Silver content has an optimum value 2% in LI and 0.5% in PD methods for achieving high photocatalytic activity. The AR88 decomposition with Ag-photodeposited method was much higher than that of deposited with LI method.

Mona et al (2008) studied morphology, optical contrast and transport characteristics of La0.7Ba0.3MnO3 (LBMO) manganite thin films bilayered with SnO_2 on Si (0 0 1) substrate, synthesized using pulsed laser deposition system. X-ray diffraction study reveals that both LBMO and SnO_2 show polycrystalline growth over the substrate. Atomic force microscopy shows interesting pyramidal structures of LBMO of size

2 μm × 1 μm × 0.1 μm. On the other hand, SnO_2 grows in the form of close packed cylindrical clusters of 200 nm radius. Near-field optical microscopy (NSOM) study using 532 nm laser reveal that optical NSOM output intensity in LBMO is four times less than SnO_2 signal. Transport characterizations show that this bilayer configuration exhibit non-linear current–voltage characteristics. The results project the system as a promising candidate in non-conventional device category in the area of spintronics.

Lin et al (2008) studied the degradation performance of 4-chlorophenol (4-CP) using TiO_2/WO_3 and TiO_2/SnO_2 systems. A BET surface area analyzer, UV–vis spectroscopy, scanning electron microscopy (SEM), X-ray diffraction (XRD) and electron spectroscopy for chemical analysis (ESCA) were employed to characterize the photocatalyst. The band edge wavelength increased to 475 nm and gap energy decreased to 2.61 eV in the TiO_2/WO_3 system as compare to the single TiO_2. Although the specific surfaces area of TiO_2/WO_3 decreases due to its larger size as compared to either TiO_2 or WO_3, the 4-CP degradation efficiency significantly increased as compared to single TiO_2 orWO_3 system at 435 nm wavelength.

Koo et al (2008) prepared the oxide semiconductor thin films by spin coating a sol-gel precursor solution based on Ga and In-co-doped ZnO (GIZO). The sol-gel-derived GIZO films were uniform and have smooth surface morphology (rms. Roughness is about 0.7 nm). The device performance of the solution-processed thin film transistors was analyzed as a function of the doping concentration and the annealing temperature. The transistors annealed at 450 °C showed clear switching behavior and output characteristic with relatively high fild effect mobility. Even when annealed at 300 °C, they showed reasonable field effect mobility and a lower threshold voltage.

Pattamatta and Madnia (2009) studied about the $Bi_2Te_3Sb_2Te_3$ nanostructures which gaining importance for use in thermoelectric applications, which is higher than conventional thermoelectric materials. $Bi_2Te_3Sb_2Te_3$ nanostructures are simulated using the Boltzmann transport equation (BTE) for phonon intensity. The phonon group velocity, specific heat, and relaxation time are calculated based on phonon dispersion model. The interfaces are modeled using a combination of diffuse mismatch model (DMM), and the elastic acoustic mismatch model (AMM). The thermal conductivity for the $Bi_2Te_3Sb_2Te_3$ superlattice is compared with the experimental data, and the best match is obtained for specularity parameter. Unlike in bulk composites, the results show a strong dependence of thermal conductivity, temperature, and heat flux on the wire size, wire atomic percentage, and interface specularity parameter.

Sharma P et al (2009) prepared visible-light sensitive bilayered photoanode of $Fe–TiO_2/Zn–Fe_2O_3$ by spray pyrolytically depositing $Zn–Fe_2O_3$ layers onto predeposited Fe–TiO2 thin film on ITO substrate. $Fe–TiO_2/Zn–Fe_2O_3$ photoelectrodes were characterized by XRD, Raman, AFM, UV-vis absorption spectroscopy. Photoelectrochemical properties of bilayered $Fe–TiO_2/Zn–Fe_2O_3$ photoelectrode were studied by Mott–Schottky curves and I–V characteristics. Bilayered $Fe–TiO_2/Zn–Fe_2O_3$ photoelectrode was observed to possess much higher separation efficiency of photogenerated charge carriers and could generate nine times better photocurrent density than pure $Fe–TiO_2$. Solar to hydrogen conversion efficiency exhibited by this electrode was 0.77%.

Yanga et al (2009) have synthesized Copper ferrite ($CuFe_2O_4$) nanoparticles via a citric acid-assisted sol–gel method. For comparison, $CuFe_2O_4$ materials were also fabricated by solid-state reaction and coprecipitation method. Techniques of XRD, TEM and UV–vis diffuse reflectance spectrum (UV–vis DRS) have been employed to characterize the as-synthesized $CuFe_2O_4$ products. The $CuFe_2O_4$ sample prepared by sol–gel approach is composed of almost uniform nanoparticles with a grain size of about 80nm and crystallized in a tetragonal crystal phase structure. Moreover, the photocatalytic activity of the as-obtained $CuFe_2O_4$ has been evaluated based on the H_2 evolution from aqueous oxalic acid solution under visible light irradiation. The effects of preparation routes, photocatalyst mass concentration, initial sacrificial reagent concentration and the durability of the as obtained $CuFe_2O_4$ have also being investigated. The best result of the photocatalytic H_2 evolution activity (1.72mmolh−1 gcat−1) was obtained over the sol–gel synthesized $CuFe_2O_4$ nanoparticles when the photocatalyst concentration is 1.0 g l−1 and the oxalic acid concentration is 0.05 M.

Dholam et al (2009) TiO_2 have synthesized by radio-frequency magnetron sputtering and sol–gel method to study the hydrogen generation by photocatalytic water splitting under visible light irradiation. Constant H_2 generation rate is obtained for long period of time by both the TiO_2 films because of the separated evolution of H_2 and O_2 gas, thus eliminating the back-reaction effect. Sputter-deposited film as compared to sol–gel-

synthesized film showed better H_2 generation rate, mainly explained in terms of the higher visible light absorption achieved by oxygen vacancies created in the TiO_2 film by the energetic target ions during deposition in pure Ar gas pressure.

Zeyan et al (2009) studied the formation of ZnO nanorod arrays on SnO_2:F (FTO) glass substrates by hydrothermal method with the addition of polyvinyl alcohol. The diameter and lengths of nanorods were controlled with PVA. The diameter of nanorods varied within 40 to 60 nm range and their length were 500 to 600 nm. PVA was regarded to play an important role during the nucleation and growth process in controlling the size and orientation of the nanorods.

Sun-kim et al (2009) used wet chemical method for the formation of ZnO upright standing nanosheets, which was based on heating an alkaline bath of Zinc Salt containing the immersed substrate. The SEM studies clearly showed the formation of two dimensional cross-linked upright standing ZnO nanosheets.

Krishna et al (2009) prepared modified cerium by impregnation method. DRS clearly shows a blue shift of 50 nm. XPS analysis of samples containing low cerium content revealed the existence of strong interaction between zeolite catalysts was evaluated in the photogeneration of hydrogen from water under UV irradiation.

Kale et al (2009) synthesized electrode of multiple band gap energy starting from wide titanium oxide to narrow range cadmium selenide by wet chemical method. The TiO_2, In_2S_2 and CdSe films were deposited one after another on ITO substrate. The overall thickness of ITO/ TiO_2/ In_2S_2/CdSe was nearly 800nm. Electrode composed of three successive descending band gap energies highlighted good absorbance in the span of visible range and better photoconversion efficiency was recorded than the bilayer.

Elijah et al (2009) developed a simple mixed metal oxide band structure (MMOBS) method to predict the electronic band structure of mixed metal oxides. Several materials in the Ti-Fe-O system that span the composition spectrum were considered in this study: anatase TiO_2, Fe-doped anatase TiO_2, limonite $TiFeO_3$, Ti-doped hematite R-Fe_2O_3, and hematite R-Fe_2O_3. The predictions by the MMOBS method for the Ti-Fe-O system were tested and confirmed using first-principles density functional theory (DFT) calculations and experimental UV-visible absorption spectroscopy measurements.

Jiaqing et al (2009) synthesized Nitrogen doped TiO_2 nanotubes with enhanced photocatalytic activity by a facile wet chemistry method. When the calcination temperature was no more than 400ºC, tubular structure was observed but when the temperature was increased, the N-TiO_2 TNTs turned into TiO_2 nanorods. The shift in the absorption edge towards higher wavelength was also observed.

Souhila et al (2009) studied the photocatalytic H_2 evolution over $CuCr_2O_4$ synthesized by nitrate route. The conductivity varied exponentially with temperature indicating an extrinsic conductivity between mixed valences states $Cr^{3+/4+}$ located in octahedral sharing common corners. The oxide exhibited p-type conductivity with an activation energy of 0.20 eV and a hole mobility of 2.14×10^{-8} cm^2/V s thermally activated. $CuCr_2O_4$ showed an excellent chemical stability. A corrosion potential of - 0.775 V_{SCE} and an exchange current density of 16 µA cm^{-2} was determined by the semilogarithm plot. The capacitance measurement (C^{-2}-V), performed in basic electrolyte, exhibited a linear behavior from which a flat band potential of 0.48 V_{SCE} was obtained. The best catalytic performance for H_2 photoproduction was obtained in (NaOH 0.5 M, $Na_2S_2O_3$ 0.025 M) with an average rate of 0.013 cm^3 h^{-1} (mg catalyst)$^{-1}$ and a quantum efficiency of 0.2% under polychromatic light.

Folusho et al (2009) used platinum nanowires mixed with tin mesotetra (4-pyridyl) porphine dichloride and nafion solution to modify the surface of glassy carbon electrode for photocurrent generation and photoelectrochemical hydrogen production. Different concentrations of porphyrin (50 mM, 100 mM, 300 mM and 500 mM) and platinum loading (200 mg/cm^2, 400 mg/ cm^2, 600 mg/cm^2 and 800 mg/cm^2) were tested at -150 mV Vs Ag/AgCl in reaction cell containing the modified glassy carbon electrode as working electrode, platinum wire as counter electrode and Ag/AgCl as reference electrode, under illumination to determine the optimum, based on photocurrent production in 50 mM potassium hydrogen phthalate buffer (pH 3) containing 0.1Na_2SO_4 as supporting electrolyte. Optimum photocurrent (12µA) was obtained at 100 mM tin porphyrin and 600 mg/cm^2 platinum loading. Detectable amount of hydrogen was produced at -350 mV Vs Ag/AgCl under irradiation with visible light which increased with increase in time.

Boumaza et al (2009) prepared spinel $ZnCr_2O_4$ for photoelectrochemical hydrogen production. The transport properties indicated p-type conductivity with activation energy of 0.21 eV. A corrosion potential of 0.404 V_{SCE} and an exchange current density of 50 $mAcm^{-2}$ was determined from the semi logarithm plot. The photocurrent onset potential, assimilated to the flat band potential, was found to be -0.39 V_{SCE}. $ZnCr_2O_4/S_2O_3^{2-}$ was a self driven system where electrons were promoted into the conduction band on absorption. A potential (-1 V) was sufficient to reduce water into hydrogen.

Patra et al (2009) synthesized stable ZnO quantum dots of 4-8 nm size by a simple solution growth technique at room temperature. Silica was used as capping agent to control the particle size as well as to achieve uniform dispersion of QDs in aqueous medium. X-ray diffractometer analysis revealed the formation of phase pure ZnO particles having wurtzite (hexagonal structures). The band gap energy of Quantum dots was found to be blue shifted as compared to bulk ZnO (3.36eV) due to quantum confinement.

Xiaoyan et al (2009) deposited ZnO–eosin Y hybrid thin films on ITO glass substrates from aqueous solutions containing zinc nitrate $Zn(NO_3)_2$ and eosin Y, using a two-step electrochemical deposition technique. Better photoelectrochemical properties were recorded for hybrid films with porous nature, exhibiting the conversion efficiency of 0.21%, open circuit photovoltage of 0.64V, and short-circuit photocurrent density of 0.67$mAcm^{-2}$ under AM 1.5 illumination.

Li-Yu et al (2009) investigated the tribological behavior of zinc oxide (ZnO) films grown on glass and silicon substrates by sol–gel method. It was found that the crystallinity was enhanced and the grain size of the ZnO films increased with annealing temperature. The ZnO films annealed at high temperature exhibited relatively low friction coefficient. Also, the wear resistance of ZnO films increased with annealing temperatures.

Yasuyoshi et al (2009) used $Ru/SrTiO_3$:Rh photocatalyst powder for H_2 evolution and varied photocatalyst powders for O_2 evolution such as $BiVO_4$ and WO_3 were suspended in acidified aqueous solutions, resulting in showing activities for water splitting without an electron mediator under visible light irradiation. The Photocatalytic activities were dependent on pH. The highest activity was found at pH 3.5. The condition of Rh doped in $SrTiO_3$ also affected strongly the Photocatalytic activity and quenching of the photoluminescence of $BiVO_4$. These results indicate that the Photocatalytic water splitting and quenching of the photoluminescence occurred through interparticle electron transfer from the conduction band of $BiVO_4$ to impurity level consisting of the reversible Rh species doped in $SrTiO_3$.

Aloney et al (2009) prepared binary films of CdSe/ZnSe on to titanium substrate byelectro-co-deposition technique in an aqueous acidic electrolyte employing different current density and deposition time duration. The photovoltaic cells are formed with these photoelectrodes. The cell configuration CdSe/ZnSe/1M NaOH-Na_2S-S/C (graphite) is used for studying the photovoltaic characteristic under illumination of 1950 lux light intensity to evaluate various cell parameters. In double layer band gap material absorb the shorter wavelength portion of the incident light and the longer wavelength portion passes to smaller band gap material and is absorbed by it. Thus, both contribute to photocurrent and larger portion of incident light is converted into electrical power.

Xunyu et al (2009) reported rational synthesis of nitrogen-doped zinc oxode nanowire arrays, and their implementation as photoanodes in Photoelectrochemical (PEC) cells for hydrogen generation from water splitting. Dense and vertically aligned ZnO nanowires were first prepared from a hydrothermal method, followed by annealing in ammonia to incorporate N as a dopants. Nanowires with a controlled N concentration (atomic ratio of N to Zn) up to ~4% were prepared by varying the annealing time. X-ray photoelectron spectroscopy studies confirm N substitution at 0 sites in ZnO nanowires up to ~4%. Incident-photon-to-current-efficiency measurements carried out on PEC cell with ZnO:N nanowires arrays as photoanodes demonstrate a significant increase of photoresponse in the visible region compared to undoped ZnO nanowires prepared at similar conditions. Mott-Schottky measurements on a representative 3.7% ZnO sample give a flat-band potential of -0.58 V.

Davood et al (2009) deposited Zinc oxide (ZnO) Thin films on microscope glass substrate by sol-gel spin coating method. Zinc acetate dehydrate was used as the starting salt material source. A homogeneous and stable solution was prepared by dissolving ZnAc in the solution of mono ethanolamine. ZnO thin films were obtained after preheating the spin coated thin films at 250^o C for 5 min after each coating. The films, after the deposition

of the eight layer, were annealed in air at temperature of 300^{o} C, 400^{o} C and 500^{o} C for 1 h. The effect of thermal annealing in air on the physical properties of the sol-gel derived ZnO thin films are studied.

Qingyue et al (2009) developed a new aqueous chemical growth method for generation of ZnO nano rod chains, transformed from ZnO micro dumbbell. The novel structure and morphology of the as-synthesized ZnO micro dumbbell and ZnO nano rod chains are characterized using X-ray diffraction and scanning electron microscopes. Field emission characterization shows that the turn-on fields for ZnO nano rod chains and micro dumbbell are 2.7 and 5.0 V/μm, respectively. The findings imply that ZnO nanorods chains may be suitable for cold-cathode electron source applications.

Sharma et al (2009) synthesized plasma surface modified nanostructure to enhance the photoelectrochemical activity of titania (TiO_2anodes). Nitrogen plasma was used to dope N at the surface of the photoanodes while removing chemisorbed species. X-ray photoelectron spectroscopy analysis showed an increase in the surface concentration of nitrogen. The photocurrent density of plasma treated samples was approximately 80% higher than that of the control. The open circuit potential of the plasma treated samples was more negative compared to that of the control, implying a favorable energetics for water splitting.

Shen et al (2010) have investigated that under microwave radiation, Ag+-doped CdS semiconductor nanocrystals with high photoluminescence quantum yield (B58%) and a surprisingly large optical window (480 to 630 nm) were formed controllably using a center-doping strategy and were optimized through a green approach in pure water solution.

Kim et al (2010) have synthesized silver doped zinc oxide nanowires on (0001) sapphire substrate by hot-walled pulsed laser deposition. Both enhancement mode and depletion mode NW field effect transistors (FETs) were fabricated. The shift of threshold voltage of silver doped zinc oxide NW FET was observed from 2.45 to -3.2 V depending on the diameter of NWs without any significant changes of the sub threshold swing, carrier concentration, and on/off ratios.

Chauhan et al (2010) synthesized nanocrystals of undoped and silver doped zinc oxide Zn1-x Ag x O (where x = 0.00 to 0.05) by coprecipitation method. Crystalline phases and optical absorption of prepared samples were determined by X-ray diffraction and UV-visible spectrophotometer. Ag doped ZnO crystallizes in hexagonal wurtzite structure. The incorporation of Ag+ in the place of Zn^{2+} provoked an increase in the size of nanocrystals as compared to undoped or pure ZnO. Optical absorption measurement indicates red shift in the absorption band edge upon Ag doping. The band gap values of as prepared undoped and doped with silver samples were found to decrease with increase in temperature from 300 to 800 ^{o}C.

Chia-Lin et al (2010) reported the thermodynamic analysis of photoelectrochemical (PEC) hydrogen production in. Because the energy required for splitting water decreases as temperature is increased, heating the system by using the long wavelength energy will increase the system efficiency. As the energy band gap of the photoelectrode increases, the induced photo-current is decreased. If photons absorbed are all excited, the maximum photo-current was 63.8 mA/cm^2. For TiO_2 (w3.2 eV) and Fe_2O_3 (w2.1 eV), the maximum photo-current is respectively 0.68 mA/cm2 and 10.4 mA/cm^2. The maximum power conversion efficiency of a PEC cell is 44.1%. For TiO_2 and Fe_2O_3, the power conversion efficiency is 2.8% and 21.9%, respectively. At 647 K and quantum efficiency ¼ 30%, the maximum hydrogen production rate is 7.5 L/m^2 h and 41.8 L/m^2 h for TiO_2 and Fe_2O_3, and the maximum efficiency of solar to hydrogen is 2.71% and 14.2% for TiO2 and Fe_2O_3 respectively. In order to increase the maximum hydrogen production rate, it is more effective to raise the quantum efficiency than raising the reaction temperature.

Wang et al (2010) have reported new layered transition metal substituted perovskite-type oxides $K_2La_2Ti_{3-x}M_xO_{10+\delta}$ (M = Fe, Ni, W; δ varies with different M) were synthesized with high-temperature solid state reaction, and characterized with X-ray diffraction (XRD) and ultraviolet–visible diffuse reflectance spectroscopy (UV–Vis DRS). The photocatalytic activity of these catalysts was studied under ultraviolet and visible light irradiation. The results indicated that substitution of a part of Ti^{4+} with Fe^{3+} and W^{6+} resulted in a marked increase in water splitting activity. The activity of these catalysts for water splitting decreased in the order: $Fe^{3+} > W^{6+} > Ni^{2+} \geq$ no substitution. The effect of different amounts of Ti^{4+} with Fe^{3+} substitution on water splitting was also evaluated. The highest hydrogen evolution was observed for perovskite composition having a

Fe:Ti molar ratio of 1:14 (1:12 weight ratio) and this hydrogen evolution was over 4 times higher than the Fe-free $K_2La_2Ti_3O_{10}$ composition. Fe was also found to be a promising component for photo activity under visible light irradiation.

Haixin et al (2010) have described a novel Photoelectrochemical (PEC) based on quantum dots (QDs) sensitized graphene for light harvesting and energy conversion. Quantum dots (QDs) sensitized graphene was prepared by in situ growth of QDS on noncovalently functionalized graphene. QDs sensitized graphene photoelectrodes showed enhanced photocurrent generation capability and incident photon-to-electron conversion efficiency (IPCE) at visible light and could also be an efficient platform for other optoelectronic applications.

Elham et al (in press) have prepared nanostructured TiO_2 hollow fibers using natural cellulose fibers as a template. This cheap and easily processed material was used to produce highly porous photoanodes incorporated in dye-sensitized solar cells and exhibited remarkably enhanced electron transport properties compared to mesoscopic films made of spherical nanoparticles. photoinjected electron life time, in particular, was multiplied by 3-4 in the fiber morphology, while the electron transport rate within the fibrous photoanode was doubled. A nearly quantitative absorbed photon-to-electrical current conversion yield exceeding 95% was achieved upon excitation at 550 nm and a photovoltaic power conversion efficiency of 7.2% reached under simulated AM 1.5 (100 m W cm^{-2}) solar illumination.

Xinjian et al (2010) found that Tantalum nitride (Ta_3N_5) has a band gap of approximately 2.07 ev, suitable for collecting more that 45% of the incident solar spectrum energy. They described a simple method for scale fabrication of highly oriented TaN_5 nanotube array films, by anodization of tantalum foil to achieve vertically oriented tantalum oxide nanotubes array structural aggregation that commonly occurs in particle films is avoided. In 1 M KOH solution, under AM 1.5 illumination with 0.5 V dc bias typical sample visible light incident photon conversion efficiencies (IPCE) as high as 5.3% were obtained. The enhanced visible light activity in combination with the ordered one-dimensional nanoarchitecture makes Ta_3N_5 nanotube arrays films a promising candidate for visible light water photoelectrolysis.

Honggang et al (2010) used DFT calculations to investigate the origin of the experimentally observed changes in the visible photoactivity of cubic and rhombic InO_3 induced by N_2 doping. Two possible mechanisms for the red shift in N-doped InO_3 are tentatively put forward, according to the doping types. For substitution N-doping models, our results show that, in both polymorphs, partial N_2p states mix with O_2p states and localized lie above the top of the valence band, acting as the frontier orbital level. Electronic transitions from these localized states induce a red shift to the visible region of the optical absorption edge. For interstitial N-doping models, NO π-antibonding stated localized in the gap contribute to the impurity levels. The electronic transition from these states may well explain the mechanism of the red shift in interstitial N-doped In_2O_3. The calculated optical properties for all N^-doped In_2O_3 show a significant visible light absorption at about 400-600 nm, photocatalyst with favorable Photocatalytic activity in the visible region.

Hua et al (2010) synthesized perovskite-like $NaTaO_3$ photocatalysts, by sol–gel and solid-state methods, loaded with NiO co-catalyst to enhance water splitting activity under UV illumination. Activity increased significantly with NiO loading and reached a maximum at 3 and 0.7 wt%, respectively, for the sol–gel and solid-state synthesized $NaTaO_3$. Beyond this point, photocatalytic activity decreased with further loading. Analysis using X-ray diffraction, high-resolution transmission electron microscopy, and diffuse reflectance spectroscopy shows that the interdiffusion of Na^+ and Ni^{2+} cations created a solid–solution transition zone on the outer sphere of $NaTaO_3$. For NiO contents less than 3 wt%, no NiO clusters appeared on the $NaTaO_3$ surface, and the reduction/oxidation pretreatment did not enhance photocatalytic activity. The high activity resulting from a low NiO loading suggests that the interdiffusion of cations heavily doped the p-type NiO and n-type $NaTaO_3$, reducing the depletion widths and facilitating charge transfers through the interface barrier.

Zhonghai et al (2010) they have reported the fabrication of lotus-root-shaped, highly smooth and ordered TiO_2 to improved the photoelectrochemical water splitting efficiency for hydrogen production nanotube arrays (TiO_2 NTs) by a simple and effective two-step anodization method. The TiO_2 NTs prepared in the two-step anodization process (2-step TiO_2 NTs) showed better surface smoothness and tube orderliness than those of TiO_2 NTs prepared in one-step anodization process. The effective photon-to-hydrogen conversion efficiency

was found to be 0.18% and 0.49% for 1-step TiO_2 NTs and 2-step TiO_2 NTs, respectively. The results suggested that the structural smoothness and orderliness of TiO_2 NTs played an important role in improving the PEC water splitting application for hydrogen generation.

Yokoyama et al (2010) have reported the effects of surface modification and reaction conditions on the photoelectrochemical properties of polycrystalline $Cu(In,Ga)Se_2$ (CIGS) thin films for water splitting. CIGS modified with platinum particles (Pt/CIGS) generated a cathodic photocurrent at potentials up to + 0.4 V vs. RHE at pH = 9.5. The photocurrent was stable for 16 h, which resulted in a turnover number of over 500. A CdS-inserted film (Pt/CdS/CIGS) had significantly improved properties compared to Pt/CIGS: a 0.3 V higher onset potential of cathodic photocurrent and a three-fold increase in the quantum efficiency. Results suggest the feasibility of CIGS as a photocathode for biphotoelectrochemical water splitting.

Dubey et al (2010) they reported anode made of multiwalled carbon nanotubes (MWNT) resulting in enhancement of exchange current density compared to graphite anode in a conventional alkaline water electrolysis cell. The hydrogen production rate with the nanotubes was measured to be $\sim$375 lh−1 m^{-2} at pH $\sim$ 14 which was nearly double of that obtained from traditional graphitic carbon electrodes at the same overpotential. This effect appears to be caused by defects on the nanotubes which reduces the energy barrier for the dissociation of OH^- into oxygen at the anode.

Lucatero and Podlaha (2010) examined AuFe electrodeposits onto a rotating disk electrode were examined to assess the composition and current efficiency behavior when citric acid, ascorbic acid, or a combination of both is present in the electrolyte. Nanowires were subsequently fabricated with pulsed current deposition to create compositionally, multilayered Au/FeAu nanowires. The FeAu layer of the nanowires was porous in a citrate electrolyte, but the porosity decreased with the addition of ascorbic acid in the electrolyte. Nonporous layers observed in the ascorbic acid bath, in combination with increased current efficiency of the deposits, suggested that a similar mechanism of Fe precipitation inside the nanorecess is less likely.

Memar et al (2010) studied the photocatalytic activity over the films surface using Fe_2O_3, WO_3 and mixture of bicomponents (Fe_2O_3:WO_3). The photo-generated of the samples were determined by measuring the currents and voltages under illumination of UV–vis light. The morphology, structure and related composition distribution of the films have been characterized by SEM, XRD and EDX respectively. Photocurrent measurements indicated surface roughness as the effective parameter in this study. The deposited surfaces by bicomponents or mixture are flat while the deposited surfaces by WO_3 appears rough. The deposited surfaces by WO_3 reveal the higher value of photocurrent measurement due to surface roughness. Indeed, the roughness can be effective in increasing contact surface area between film and electrolyte and diffuse reflection (light scattering effect). The solution (Fe_2O_3:WO_3) shows the low photocurrent value in compare to WO_3 and Fe_2O_3 hat it may be due to decomposition the compound at 450 ± 1°C to iron-tungstate $Fe_2(WO_4)_3$.

Dholam et. al. (2010) synthesized Cr-doped-TiO_2 thin films, with three different Cr concentrations (2, 5.5, and 9 at.%) by radio-frequency magnetron sputtering in order to sensitize TiO_2 in visible light. Negligible photocurrent was measured with Indium Tin Oxide (ITO)/Cr-doped-TiO2 (9 at.%) single bilayer sample due to the increased recombination rate of the photo-generated charges on the defects associated to the Cr^{3+} ions. To lower the charge recombination rate in the Cr-doped-TiO_2, multilayer films with different numbers of ITO/Cr-doped-TiO_2 bilayers were deposited by keeping the total thickness of TiO_2 constant in each multilayer film. When the multilayer films were exposed to visible light, they were observed that the photocurrent was found to increases as function of the number of bilayers by reaching the maximum with 6-bilayers of ITO/Cr-doped-TiO_2. The superior photocatalytic efficiency of the 6-bilayers film implies higher hydrogen production rate through water-splitting.

Li et al (2010) prepared ZrW_2O_8 by hydrothermal reaction process with band gap energy of 4.0 eV. The average rate of H_2 evolution over 0.3wt% Pt/ZrW_2O_8 in the presence of CH_3OH as electron donor (ED) was 23.4 μmol/h, while the average rate of O_2 evolution over ZrW_2O_8 in the presence of $AgNO_3$ as electron scavenger (ES) was 9.8 μmol/h. Moreover, H_2 was evolved over 0.3 wt% Pt/ZrW_2O_8 from pure water splitting at a rate of 5.2 μmol/h. The study indicated that the band structure of ZrW_2O_8 was found to be suitable for reducing H^+ to H2 and oxidizing H_2O to O_2. The band structure and photocatalytic water splitting properties of ZrW_2O_8,

different from either ZrO_2 (5.0 eV) or WO_3 (2.7 eV), were attributed to the hybridization of W5d and Zr_4d in conduction band (CB) as well as the change in crystal structure.

Yue et al (2011) developed a simple soft-chemical method of doping Zn into g-C_3N_4 to prepare a metal-containing carbon nitride. The doping was confirmed by x-ray photoelectron spectroscopy, and diffusion reflectance spectra revealed a significant red shift in the absorption edge of Zn/g-C_3N_4. This hybrid material shows high photocatalytic activity and good stability for hydrogen evolution from an aqueous methanol solution under visible light irradiation (> 420 nm). The hydrogen evolution rate was more than 10 times higher for a 10%-Zn/g-C_3N_4 sample (59.5μmol h−1) than for pure g-C_3N_4. The maximum quantum yield was 3.2% at 420 nm.

Li et al (2011) achieved a high efficiency of the photocatalytic H_2 production using graphene nanosheets decorated with CdS clusters as visible-light-driven photocatalysts. These nanosized composites reached a high H_2-production rate of 1.12 mmol h-1 (about 4.87 times higher than that of pure CdS nanoparticles) at graphene content of 1.0 wt % and Pt 0.5 wt % under visible-light irradiation and an apparent quantum efficiency (QE) of 22.5% at wavelength of 420 nm. This high photocatalytic H2-production activity is attributed predominantly to the presence of graphene, which serves as an electron collector and transporter to efficiently lengthen the lifetime of the photogenerated charge carriers from CdS nanoparticles.

Mukherji et al (2011) studied a new type of nitrogen-doped tantalum tungstenate ($CsTaWO_6$) material, which demonstrates excellent visible light absorption and improved photocatalytic activity. XRD patterns reveal that the defect pyrochlore-type structure of $CsTaWO_6$ remained intact upon nitrogen doping. UV-vis spectra indicate that nitrogen doping in the compound results in a red-shift of the absorption edge from 358 nm to 580 nm, thus offering significantly increased visible light absorption. XPS further indicates that [Ta/W]–N bonds were formed by inducing nitrogen to replace a small amount of oxygen in the material, resulted in a compound of $CsTaWO_6$−N. The explanation of the experimental results was supported by density functional theory calculations. The bandgap reduces significantly from 3.8 to 2.3 eV due to N_2p and O_2p orbital mixing. The role of the new N_2p states is also investigated by studying the production of the •OH radicals in the visible light region (420 nm). Compared with its undoped counterpart, nitrogen-doped $CsTaWO_6$−N exhibits a nearly 100% increase in solar hydrogen production efficiency.

Liu et al (2011) studied plasmonic enhancement of photocatalytic water splitting under visible illumination by integrating strongly plasmonic Au nanoparticles with strongly catalytic TiO_2. The photocatalytic splitting of water in TiO_2 with the addition of Au nanoparticles enhanced under visible illumination. Electromagnetic simulations indicate that the improvement of photocatalytic activity in the visible range is caused by the local electric field enhancement near the TiO_2 surface, rather than by the direct transfer of charge between the two materials. Here, the near-field optical enhancement increases the electron-hole pair generation rate at the surface of the TiO_2, thus increasing the amount of photogenerated charge contributing to catalysis.

Kumar and Devi (2011) underlined the general aspects of PEC by taking titania as a photocatalyst. However, the large band gap of titania and massive recombination of photogenerated charge carriers limit its overall photocatalytic efficiency. The former can be overcome by modifying the electronic band structure of titania including various strategies like coupling with a narrow band gap semiconductor, metal ion/nonmetal ion doping, codoping with two or more foreign ions, surface sensitization by organic dyes or metal complexes, and noble metal deposition. The latter can be corrected by changing the surface properties of titania by fluorination or sulfation or by the addition of suitable electron acceptors besides molecular oxygen in the reaction medium. Encompasses several advancements made in these aspects, and also some of the new physical insights related to the charge transfer events like charge carrier generation, trapping,detrapping, and their transfer to surface are discussed for each strategy of the modified titania to support the conclusions derived. A recent venture on the synthesis and applications of anatase titania with a large percentage of reactive {001} facets and their band gap extension to the visible region via nonmetal ion doping is also discussed.

Junga et al (2011) worked on graphene-coated Al_2O_3 (GCA)-TiO_2 nanocomposite photoanodes fabricated by dispersing the GCA (1, 3, and 5 wt. %) and TiO_2 nanoparticles. Photoelectrochemical (PEC) responses under the white light illumination were significantly enhanced with the increase of the GCA content and all of the

GCA-TiO_2 films exhibited much better PEC responses than the electrode prepared from the TiO_2 alone. The significantly improved PEC response of the GCA-TiO_2 can be attributed to the enhanced electron transport.

Esmaili et al (2011) prepared NiFe/Cu multilayers which were deposited from a single bath in the potentiostatic mode using two different solutions. The layers were characterized by the layers, SEM, HRTEM, XRD and AFM. SEM results revealed the layered structure of the deposits for relatively thick bilayers. While HRTEM provided direct evidence for the composition modulation across successive layers in the NiFe/Cu nanometer-multilayered structure prepared from solution B.

Dussan et al (2011) studied the magnetic properties of $BiFeO_3$ (BFO)-CoFe2O4 (CFO) heterostructure thin films, grown on (STO) substrates by employing pulsed laser deposition (PLD) method. The XRD patterns of BFO-CFO multilayer thin films compared with the pure CFO and BFO thin films grown using under identical conditions evidenced that all peaks present correspond to CFO and BFO structure in two separate phases. The anomalous enhancement in magnetization has been observed for BFO−CFO multilayer thin films, relative to pure BFO thin films in all three different orientations. The saturation magnetization for (100), (111) and (110) oriented BFO-CFO thin films are 44, 62 and 80 emu/cc suggested that (110) was most preferable direction to achieve the magneto electric (ME) coupling effect.

Li et al (2011) prepared the graphene/TiO_2 composite film on the glass plate by dipping-lifting in sol–gel solution and reducing process. Then, the Ag/graphene/TiO_2 composite film was fabricated by interface reaction with $AgNO_3$ and $N_2H_4{\cdot}H_2O$ on the surface of graphene/TiO_2 composite film. The characterization results show that the uniform porous TiO_2 film is made up of the anatase crystal, and the Ag/graphene/TiO_2composite film is constructed by doping or depositing graphene sheets and Ag nanoparticles on the surface of TiO_2 film. The photoelectrochemical measurement results indicate that the Ag/graphene/TiO_2 composite film has an excellent photoelectrochemical conversion property.

Tokarz et al (2011) prepared NiFe/Cu multilayer films which have been electrodeposited potentiostatically on (001)-oriented Si and polycrystalline Cu substrates by a single bath technique. Standard error of mean results reveals the layered structure of deposits for relatively thick bilayer thickness (ca. approximately 200 nm). The modulated structure of NiFe/Cu multilayers with extremely thin bilayer thickness (nominal period Lambda= 8 nm) was investigated by transmission electron microscope techniques. A columnar structure of the deposit with column diameter in the range from 10 to 30 nm was observed. Results were compared with X-ray diffraction measurements of crystallites size obtained by Scherer equation. The line scans acquired using EDS confirmed the layered structure of the deposit, but pointed towards possibility of intermixing of species from alternating sublayers especially in case of those with finer period.

Liu et al (2011) proposed a novel interdigital electrode/WO_3/TiO_2 heterojunctional-electrical layered (HEL) system which is better to enrich the holes in the surface of a material system. The HEL system consists of interdigital electrode, WO_3 layer and TiO_2 layer, and they are orderly printed onto the alumina substrate from bottom to top using the technology of screen printing. It is surprise that the synergistic effect of layered heterojunction and external low bias can strengthen the separation of electron-hole pairs in both TiO_2 and WO_3, and enrich the TiO_2 surface layer with photogenerated holes to degrade the gaseous pollutants. In comparison with the pure TiO_2 film, a 6-fold enhancement in photocatalytic activity was observed using the HEL system by applying a very low bias of 0.2V. The results also showed that the remarkable improvement could not be obtained when either the WO_3 layer or the low external bias was absent.

Biswal et al (2011) prepared a novel composite CdS–ZnS/ZTP photocatalyst working under visible light by a two-step sulfidation procedure. The photocatalytic activity of the cadmium sulfide–zinc sulfide supported composite catalyst was evaluated toward hydrogen energy production in the presence of hole scavenger, sulfide and compared with the activity of neat CdS, ZnS, ZTP, CdS–ZnS, CdS/ZTP and ZnS/ZTP without using any co-catalyst. The photocatalysts were characterized by X-ray diffraction (Small Angle X-ray diffraction Studies and Broad-Angle XRD, N_2 adsorption–desorption, DRUV-vis, PL, SEM/EDX, XPS, TEM etc. Amongst all the catalysts, 5CdS–ZnS/ZTP showed highest results toward hydrogen production under visible light illumination.

Hou et al (2011) synthesized three-dimensional (3D) multicomponent oxide, $Bi_{12}TiO_{20}/TiO_2$ hierarchical heterostructure via a one-step and template-free hydrothermal route. X-ray diffraction and X-ray photoelectron

spectroscopy measurements confirm that the composition of the as-fabricated sample is Bi_12TiO_{20}/TiO_2 composite. Scanning and transmission electron microscopy observation reveals that the as-synthesized sample is microsized flower-like hierarchical networks consisted of $Bi_{12}TiO_{20}$ nanorods decorated with the primary TiO_2 nanoparticles. Extension of the light absorption from the ultraviolet region to the visible-light region was confirmed by UV-vis absorption spectra. Due to the structure-property relationships, the 3D $Bi_{12}TiO_{20}/TiO_2$ heterostructure exhibited enhanced visible photocatalytic activity over that of $Bi_{12}TiO_{20}$ and TiO_2 samples in the decomposition of Rhodamine B in water which is a typical model pollutant. The effective separation of photogenerated carriers driven by the photoinduced potential difference generated at the $Bi_{12}TiO_20/TiO_2$ junction interface, demonstrating that the $Bi_{12}TiO_{20}/TiO_2$ heterostructure is a promising candidate as a visible light photocatalyst.

Kronawitter et al (2011) studied a perspective on the design of all-oxide heterostructures for application in photoelectrochemical cells for solar water splitting. In this a novel hetero-nanostructure array, based on quantum-confined and visible light-active iron (III) oxide nanostructures and their surface modification with tungsten (VI) oxide, was introduced. The heterostructure architecture wass designed to combine the functionality of the consituent phases to address the primary requirements for electrodes enabling the efficient generation of hydrogen using solar energy: visible light activity, chemical stability, appropriate bandedge characteristics, and potential for low-cost fabrication. Photoelectrochemical characterization for solar hydrogen/oxygen generation indicates the presence of unexpected minority carrier transfer dynamics within the oxide hetero-nanostructures, as observed additionally by ultrafast transient absorption spectroscopy.

Murph et al (2011) presented recent advances in synthesis, characterization, optical, catalytic and physico-chemical properties of nanoscale materials with potential applications in fuel cells processes. In particular, this review and original research focuses on the catalytic properties of noble metal nanoparticles (e.g., platinum, gold and silver) as a function of particles morphology and composition (e.g., isotropic and anisotropic, solid, hollow and core-shell structures, and mono- and bi- metallic compositions, supported and unsupported).

Ling et al (2011) have synthesized Sn-doped hematite nanowires and nanocorals on a fluorine-doped tin oxide (FTO) substrate by a hydrothermal method and studied their implementation as photoanode for photoelectrochemicalwater splitting. X-ray photoelectron spectroscopy analysis confirmsed substitution at sites in hematite. Sn dopant serves as an electron donor and increases the carrier density of hematite nanostructures. The hematite nanowires sintered at 800°C yielded a pronounced photocurrent density of 1.24 mA/cm^2 at 1.23 V vs RHE, which is the highest value observed for hematite nanowires while Sn-doped hematite nanocorals showed a remarkable photocurrent density of 1.86 mA/cm^2 at 1.23 V vs RHE, which is approximately 1.5 times higher than that of the nanowires.

Wirth et al (2011) investigated the adsorption and splitting of the water molecule by light and/or an external potential using a rutile ruthenium dioxide anode. Periodic density functional calculations, were used to find the structure of adsorbed H_2O molecules and radicals involved in the splitting process (O, OH, OOH) and compared with the available experimental results. On the basis of these electronic-structure calculations, a method was used to calculate the stability of the reaction intermediates and conclude on the thermodynamical possibility of the water splitting reaction at the surface. Results showed that a moderate overpotential of 0.64V is required for the reaction to take place at the RuO_2 (110) surface.

Grimes et al (2011) reported splitting of water on a novel heterojunction $WO_3/BiVO_4$ photoanode The heterojunction films were prepared by solvothermal deposition of a WO_3 nanorod-array film onto fluorine-doped tin oxide (FTO) coated glass, with subsequent deposition of a low bandgap, 2.4 eV, visible light responding $BiVO_4$ layer by spin-coating. The heterojunction structure offers enhanced photoconversion efficiency and increased photocorrosion stability due to the high surface area and improved separation of the photogenerated charge at the $WO_3/BiVO_4$ interface.

Ashkarran et al (2011) synthesized Ag-doped TiO_2 nanoparticles by combination of two bottom-up and top-down methods and characterized by XRD, BET, XPS and ultra violet-visible absorption spectroscopy UV-Vis. The anti- bacterial activity was tested against Escherichia coli (E-coli). The results revealed that the Ag/TiO_2 nanoparticles extended the light absorption spectrum toward the visible region and significantly enhanced the inactivation of E-coli bacteria under visible light irradiation. The significant enhancement in the antibacterial

properties of Ag/TiO_2 nanoparticles under visible light irradiation was ascribed to the effect of doped noble metal Ag by acting as electron traps in TiO_2 band gap.

Saikia et al (2011) prepared thin films of CdS quantum dot (QD) embedded in PVA matrix. Silver was doped into CdS/PVA thin film by adding silver nitrate into cadmium acetate with cadmium to silver ion ratio 103:1. The films were characterized by XRD, SEM, TEM, and UV-Visible and photoluminescence spectroscopy. The results indicated that films were nanocrystalline in nature, highly transparent, homogeneous with no visible pinholes and suitable for solar cell application. Doping of silver into CdS/PVA nanocomposite thin film has improved the conversion efficiency of the cell from 4.92% to 5.63%.

Zeferino et al (2011) studied the effects of Ag doping on the crystallinity and optical properties of zinc oxide nanoparticles have been studied by x-ray diffraction, diffuse reflectance spectroscopy, micro-Raman, and photoluminescence spectroscopy. Result showed that Ag-doping at low concentration improves the optoelectronic properties of ZnO nanostructures, Ag-doping at high concentrations drastically modify the emission behavior and lattice vibrational characteristics of the nanostructures. High Ag content in ZnO nanostructures causes lattice deformation, induces silent vibrational modes in Raman spectra, and reduces excitonic UV emission due to concentration quenching

Hamedani et al (2011) reported the fabrication and photoelectrochemical properties of highly ordered Sr-doped TiO_2 nanotube arrays synthesized via a one-step electrochemical anodization technique. The morphology and quality of the fabricated materials were found to be significantly affected by the pH of the electrolyte as well as the solubility limit of $Sr(OH)_2$ in the test electrolyte. The photoelectrochemical measurements revealed that Sr doping can significantly improve the photoconversion efficiency of the material. Using Sr-doped TiO_2 nanotube arrays, an electrode photoconversion efficiency of 0.69% was obtained, which is more than 3 times higher than that of the undoped nanotube arrays (0.2%) fabricated and tested under the same conditions.

Oszajca et al (2011) prepared nanocrystalline titanium dioxide on which ruthenium complexes [Ru(trpy)L], [Ru-$(bpy)_2$L], and [Ru$(dcbpy)_2$L] were chemisorbed. The resulting materials were sensitive to visible light. Photoelectrochemical studies revealed significant, potential-dependent photosensitization in the 300 - 650 nm window. The direction of the photocurrent could be switched from cathodic to anodic and vice versa by application of adequate external potential which were predicted by photoelectrochemical, spectroscopic and theoretical studies.

Su et al (2011) reported novel heterojunction $WO_3/BiVO_4$ photoanode for photoelectrochemical water splitting. The heterojunction films were prepared by solvothermal deposition of aWO_3 nanorod-array film onto fluorine-doped tin oxide (FTO) coated glass, with subsequent deposition of a low bandgap, 2.4 eV, visible light responding $BiVO_4$ layer by spincoating. The heterojunction structure offered enhanced photoconversion efficiency and increased photocorrosion stability. Compared to planar $WO_3/BiVO_4$ heterojunction films, the nanorod-array films show significantly improved photoelectrochemical properties due which improved separation of the photogenerated charge at the $WO_3/BiVO_4$ interface.

Qin et al (2011) synthesized controlled growth of highly ordered, [211]-oriented FeOOH nanowire arrays on various substrates, such as Pt,W, Ti, and fluoride-doped tin oxide (FTO) glass which was achieved by a solvothermal method in aqueous acetonitrile solutions at 80° and 120° C, followed by annealing to form α-Fe2O3 nanowires with their [110] direction perpendicular to the substrate. Adjusting the reaction pH and temperature enabled control of the nanowire length. The pH has a dramatic effect on the nanowire growth, with low pH resulting in the growth of longer wires because of the acid-catalyzed hydrolysis of acetonitrile. Photoactive hematite was prepared by diffusing Ti or Sn into the nanowires during thermal annealing. The Ti- and Sn-doped one-dimensional [110]-oriented α-Fe2O3 nanowire arrays provided an effective pathway for electron transport, demonstrating increased photocurrents, up to 1.3 mA/cm^2 under air mass 1.5 global (AM 1.5G) illumination, in photoelectrochemical water oxidation.

Zhang et al (2011) reported partially hydrolyzed aluminum phthalocyanine chloride (denoted as AlPc) for visible-light-responsive photoelectrochemical and photocatalytic properties of nanoparticles of C_{60}. The three types of nanoparticles were obtained through a reprecipitation method from N-methyl-2-pyrrolidone solutions

of C60, aluminum phthalocyanine chloride (AlPcCl), and their mixture, respectively. The nanoparticle composite's ultraviolet-vis absorption, diffuse reflectance and FTIR spectra, XRD pattern, and SEM image are all similar to the sum of those of the C60 and AlPc particles, respectively. The nano-ordered composite exhibit p/n junction like photoelectrochemical characteristics which were investigated in comparison with the vapor-deposited C60 (n-type). The nanoparticle composite further shows photocatalytic activity for the decomposition of trimethylamine to carbon dioxide in a suspension system.

Mao et al (2011) synthesized vertically aligned hematite nanorod and nanotube arrays on a conductive substrate by the electrochemical deposition method with the help of an anodized aluminum oxide nanotemplate. The two types of nanostructured hematite were used as the photoanode for photoelectrochemical cells. The hematite nanotubes exhibited much higher photoelectrochemical activity than the hematite nanorods, including an improved photocurrent density, more negative onset potential, better photon harvesting, and better charge carrier transfer ability.

Riha et al (2011) synthesized Cu_2ZnSnS_4 (CZTS) nanocrystals by a hot injection solution method which has been fabricated into thin films by dip-casting onto fluorine doped tin oxide (FTO) substrates. The photoresponse of the CZTS nanocrystal films was evaluated using absorbance measurements along with photoelectrochemical methods in aqueous electrolytes. Photoelectrochemical characterization revealed a p-type photoresponse, film thickness, and low-temperature annealing on the photocurrents from front and back illumination suggest that the Minority carrier diffusion and recombination at the back contact are the main loss mechanisms in the cell. Low-temperature annealing resulted in significant increases in the photocurrents for films made from both Zn-rich and stoichiometric CZTS nanocrystals.

Lee et al (2011) modified the fabrication of a superhydrophobic nanocoating through a simple spin-coating and chemical. The resulted coated surface displayed a static water contact angle and contact angle, showed excellent superhydrophobicity. The surface wet ability could be modulated by the number of ZnO nanoparticle coating cycles, which in turn affected surface roughness. Because of its surface-independent characteristics, this method could be applicable to a wide range of substrates including metals, semiconductors, papers, cotton fabrics, and even flexible polymer substrates. This super hydrophobic surface showed high stability in thermal and dynamic conditions, which are essential elements for practical applications. Furthermore, the reversible switching of wetting behaviors from the superhydrophilic state to the superhydrophobic state was demonstrated using repeated chemical modification/ heat treatment cycles of the coating films.

Lee et al (2011) described the morphology-controlled synthesis of three-dimensional (3D) ZnO nanoarchitectures via a facile hydrothermal route. In this approach, vertical and inplane crystallographic orientations of ZnO crystals were tuned by appropriate patterning of growth masks and seed layer control, which enabled the formation of three types of ZnO nanoarchitectures. If polycrystalline ZnO layers with poor c-axis orientation were used as a seed, flower-like ZnO nanoarchitectures composed of radially oriented ZnO nanorods were achieved. In the case of c-axis oriented ZnO seeds, polygonal ZnO pillars grew vertically at the center of the growth holes. These morphology-controlled ZnO nanoarchitectures exhibited clear differences in light propagation characteristics, which could be ascribed to strong light guiding in the one-dimensional nanostructures.

Shinagawa et al (2011) reported on a versatile and low-temperature solution process to grow vertical and dense ZnO nanorod arrays. The ZnO nanorod arrays have been deposited by immersing a Pd-nanoparticle-coated substrate into an aqueous solution containing Zn(NO3)2 and dimethylamineborane (DMAB). Coating substrates with Pd nanoparticles that act not only as a catalyst for DMAB oxidation but also as a ZnO nucleation seed layer allows similar ZnO nanorod arrays to be deposited on different types of substrates such as glass and PET. The effect of deposition conditions on the resulting ZnO morphology was examined, and the size (length and diameter) of ZnO nanorods is demonstrated to be controllable independently by just adjusting the Zn(NO3)2 concentration and deposition time. The degree of c-axis orientation wass evaluated in terms of the texture coefficient and its standard deviation, and all samples show a high vertical alignment irrespective of the Zn(NO3)2 concentration and deposition time. As-grown ZnO nanorod arrays exhibit UV and visible light emission at room temperature, and interstitial oxygen was found to be a major lattice defect.

Biswas et al (2012) obtained different morphologies of WO_3 nanocrystals such as nanorods and nanoplates which have been obtained under hydrothermal conditions using ammonium meta tungstate as the precursor in presence of different organic acids such as citric, oxalic, and tartaric acid in the reaction medium. Samples were characterized for the crystal structure, particle morphology, and optical band gap of the synthesized powders have been done by XRD, TEM, SEM and solid state UV–visible spectroscopy. The as-synthesized materials were WO_3 hydrates with orthorhombic phase which transformed to the hexagonal WO_3 through dehydration upon heating at 350 °C. The photocurrent measurements upon irradiation of light exhibited photocurrent of about 0.77, 0.61, and 0.65 $mAcm^{-2}$ for theWO_3 film derived with the oxalic acid, tartaric, and citric acid assisting agents at 1.8 V versus Ag/AgCl electrode.

Logar et al (2012) synthesized nanostructured, γ-Al_2O_3/TiO_2 composite powder. This was used in the formation of a nanostructured TiO_2 layer on the surface of the γ-Al_2O_3 lamellas. Transmission electron microscopy TEM, XPS and XRD were employed to evaluate the morphology, the chemical composition and the crystallinity of the γ-Al_2O_3/TiO_2 particles of the composite powder. The as-formed, nanostructured, γ-Al_2O_3/TiO_2 composite powder exhibited a 2.7-times-higher photo-activity in the near-UV region compared to commercially available TiO_2 (Degusa P25), as monitored by the photo-decomposition of a methylene blue (MB) dye.

Jiang et al (2012) worked for better performance of dye sensitized solar cells (DSSCs), a bilayer structured electrode was constructed by employing a mesoporous anatase TiO_2 overlayer above a commercial P25 TiO_2 nanoparticles underlayer. The mesoporous anatase TiO_2, prepared through a facile surfactant-assisted sol–gel process, possessed large pore size and well inter-connected network structure. The dye adsorption capability of the mesoporous TiO_2 was nearly twice that of the P25 counterpart. In the electrode, the mesoporous TiO_2 film enhanced both dye adsorption and light-harvest, to increased photocurrent (Jsc). Compared to the single P25 TiO_2 film, the synergy of the mesoporous TiO_2 and the P25 TiO_2 nanoparticle films in the electrode resulted in a 24% improvement in light-to-electricity conversion efficiency.

Tong et al (2012) focused on the scientific and technological possibilities offered by photocatalytic materials. The study begins with a survey of efforts to explore suitable materials and to optimize their energy band configurations for specific applications was also examined the design and fabrication of advanced photocatalytic materials in the framework of nanotechnology. Many of the most recent advances in photocatalysis have been realized by selective control of the morphology of nanomaterials or by utilizing the collective properties of nanoassembly systems. It also highlights the current theoretical understanding of aspects of photocatalytic materials and crucial issues that should be addressed in future research activities.

Vercelli and Zotti (2012) were investigated Oligo(poly)thiophenes by photoelectrochemical methods as monolayer sensitizers of CdSe nanocrystal (CdSe-NCs) and TiO2 polycrystalline films on ITO electrodes. 7.5 nm diameter CdSe-NCs layers and polycrystalline anatase TiO2 films were functionalized with dicarboxylic sexithiophene and with two polythiophenes. The modified electrodes were investigated in a three-electrode photoelectrochemical cell in the presence of iodide as sacrificial generator of intense and steady oxidative photocurrents. The oligo(poly)thiophenes act in general as moderate hypersensitizers (roughly twice more efficient than calculated). Poly(thiophene-3-propionic acid) monolayers, formed on CdSe-NC structures from ethanol, which generate a strong hypersensitization, i.e., a response 5 times higher than expected.

Wong et al (2012) investigated the effect of ZnO nanoparticle properties on the dye-sensitized solar cell performance. Nanoparticles with different sizes and optical properties were considered for their complex relationship between native defects, dye adsorption, charge transport and solar cell performance. The presence of a high concentration of nonradiative defects was found to be detrimental to photovoltaic performance, whereas for radiative defects, samples displaying orange-red defect emission exhibited better performance compared to samples with green defect emission (when the samples had similar emission intensities).

Li et al (2012) investigated one-dimensional oxide nanostructure arrays as photoelectrodes in solar cells for which it is highly desirable for the electrode to have a broad light absorption and an efficient charge separation. In this work ZnO core−shell nanowire array wass prepared through temperature- gradient CVD of ZnxCd1−xSe layer onto the pregrown ZnO nanowires. The core−shell nanowire array photoelectrodes yielded a continuous absorption edge from 2.7 (460 nm) to 1.77 eV (700 nm) across the sample surface. The core−shell heterostructure facilitates the photogenerated electron−hole pair separation and the electron transfer from

ZnCdSe to ZnO. By using such core−shell nanowire arrays as photoanodes for solar hydrogen generation via a PEC cell, a photocurrent density of $\sim$5.6 mA/cm^2 was achieved under 1 sun solar light illumination at zero bias versus Ag/AgCl.

Dong et al (2012) investigated ZnO nanowires at high pressures of up to 27 GPa in situ in a diamond anvil cell using synchrotron X-ray diffraction. Upon compression, a wurtzite to rocksalt phase transformation was observed, this transformation were enhanced compared with all previously studied morphologies of ZnO, including nanocrystals and their bulk counterparts. The rocksalt phase was found to sustain at near ambient pressure and could be recovered in a significant amount. The SEM images of the ZnO nanowires both before and after the compression suggest the pressure-induced morphology modifications. Pressure-induced phase transition mechanisms were explored by examining the cell parameters and the internal structural parameter with pressures.

Sun et al (2012) designed and fabricated a novel semiconductor-sensitized solar cell using a poly (3-hexylthiophene) (P3HT)/CdS/ZnO coreshell nanotube array as the photoanode. A facile sequent electrodeposition process was employed to prepare the photoanode. The one-dimensional three-component coreshell ordered nanoarray structure was formed by electrodepositing CdS nanoparticles and a thin P3HT layer onto the walls of ZnO nanotubes, which enhanced the optical absorption in the visible region and presented an interface between n-type CdS and p-type P3HT to improve the charge separation. An energy conversion efficiency up to 1.28% was obtained with the designed nanostructured solar cell based on the P3HT/CdS/ZnO nanotube array.

Barpuzary et al (2012) synthesized Nanourchin-shaped narrow-band-gap semiconductor photocatalysts with high surface area which resulted in effective photocatalysis. The impregnated growth of 1D CdS nanowires onto Al2O3 and ZnO templates as cores generated novel urchinlike morphology of CdS/oxide photocatalysts. The CdS/Al2O3 and CdS/ZnO nanourchins enhanced hydrogen generation with apparent quantum yields (AQY) of 11% and 15%, respectively. Mechanistically, the template-based CdS influenced the photocatalytic activity in two ways: (i) direct well-dispersed growth of CdS onto the oxide core, leading to a high surface area for enhanced light absorption, and (ii) charge transfer from the conduction band of highly crystalline CdS to that of the oxide, which facilitate efficient charge separation for hydrogen production. These two mechanisms, a simple, low-cost, and environmentally friendly hydrothermal strategy were employed to synthesized novel nanourchin-shaped CdS-based heteroarrays. This new morphology stimulates the surface area per unit volume of the photocatalyst for photocatalytic water splitting.

References

Ashkarran A (2011) *J. Theoretical Applied Physics*, **4**, 1-8.

Aloney R K, Dongree J K, Chandra B P and Ramakhiani M (2009) *Chalcogenide Lett.*, **6**, 569-575.

Antonio C, Vanga R R, Marieke K V V, Ruud E I S and Gion C (2004) *Photochem. Photobiol. Sci.*, **3**, 1017–1025.

Arena D N, Saitta G, Galvagno S, Milone C and Pistone A (2008) *Microelectronics J.*, **39**, 1659–1662.

Aroutiounian V M, Arakelyan V M, Shahnazaryan G E, Hovhannisyan H R, Heli W and John A T (2007) *Solar Ene.*, **81,** 1369–1376.

Aroutiounian V M, Arakelyan VM and Shahnazaryan G E (2005) *Solar Ene.*, **78**, 581–592.

Biswas S K, Baeg J O, Moon S J, Kong K J, So W W and Res J N (2012), *J. Nanopart. Res.*, 14:667

Biswal N, Das D P, Martha S, Parida K M (2011), *Int. J. Hydrogen Ene.*, **36**, 13452-13460.

Badawy W A (1997) *J. of Mat. Sci.*, **32,** 4979 – 4984.

Balamurugan B and Mehta B R (2001) *Thin Solid Films*, **396**, 90.

Balamurugan B, Mehta B R, Avasthi D K, Singh F, Arora A K, Rajalakshmi M, Raghavan G, Tyagi A K and Shivprasad S M, (2002) *J. Appl. Phys.*, **92,** 3304.

Bernal M E P, Casero R J R and Rives V (2004) *Solid State Chem.*, **48**,145

Bassekhouad Y, Trari M and Doumerc J P (2003) *Int. J. Hydrogen Ene.*, **28**, 43.

Bjorn M, Miller E L, Daniela P R and Rocheleau E (2007) *Int. J. Hydrogen Ene.*, **32**, 3110 – 3115.

Borgohain K, Murase N and Mahamuni S (2002) *J. Appl. Phys.*, **92**, 1292-1297.

Boumaza S, Bouguelia A, Bouarab R and Trari M (2009) *Int. J. Hydrogen Ene.*, **34**, 4963-4967.

Behnajady M A, Modirshahla N, Shokri M, Rad B (2008) *J. Global Nest*, **10**, 1-7.

Barpuzary D, Khan Z, Vinothkumar N, De M and Qureshi M (2012), *J. Phys. Chem. C*, **116**, 150–156.

Crabtree G W and Dresselhaus M S (2008), *MRS Bull.*, **33**, 421-428.

Currao A (2007), *Chimia.*, **61**, 815-819.

Changdong G, Jun L, Jianshe L and Guoqu Z (2007) *Applied Surface Sci.*, **253,** 7011-7015.

Che-Chia H, Jun-Nan N and Hsisheng T (2008) *Solar Ene. Mat. and Solar cells*, **92**, 1071-1076.

Chengkun X, Yasser A S, Ingler W B and Khan S U M (2007) *Solar Ene. Mat. & Solar Cells*, **91,** 938-943.

Chauhana R, Kumar A and Chaudhary R P (2010) *Archives Applied Sci. Research*, **2,** 378-385.

Chia-Lin T, Chung-Jen T and Jyh-Chen C (2010) *Int. J. Hydrogen Ene.*, **35**, 2781-2785.

Davood R., Taha R (2009) *Applies Surface Sci.*, **255**, 5812-5817.

Debnath N C and Anderson A B (1982) *J. Electrochem. Soc.*, **129**, 2169-2174.

Dholam R, Patel N, Adami M, and Miotello A (2008) *Int. J. Hydrogen Ene.,* **33**, 6896-6903.

Drobny V F and Pulfrey L (1979) *Thin Solid Films*, **61**, 89-98.

Dubey P K, Sinhab A S K, Talapatrac S, Koratkard N, Ajayane P M and Srivastava O N (2010) *Int. J. Hydrogen Ene.*, **35**, 3945-3950.

Dholam R, Patel N, Santini A and Miotello A (2010), *Int. J. of Hydrogen Ene.*, **35**, 9581–9590.

Dholam R, Patel N, Adami M and Miotello A (2009), *Int. J. of Hydrogen Ene.*, **33**, 6896–6903.

Dong Z, Zhuravlev K K, Morin S A, Li L, Jin S and Song Y (2012), *J. Phys. Chem. C, **116**, 2102–2107*.

Dussana S, Singhb M K and Katiyar R S (2011), Integrated Ferroelectrics: An Int. J., **124**, 73-78.

Elham G, Nima T, Shaiik M.Z, Michael G and Jacques-E M (2010), *Nano Letters*, **10**, 1632-1638.

Elijah T, Subhashis B, Cynthia S L and Pratim B (2009) *J. Phys. Chem. C*, **113**, 2014–2021.

Eun Y K, Jong H P and Gui Y H (2008) *J. Power Sources*, **184**, 284-287.

Evic K, Dubc ek P, Duguay S, Zorc H, Radic N, Pivac B, Slaoui A and Bernstorff S (2007), Physica E: Low-dimensional Systems and Nanostructures, **38**, 50–53.

Esmaili S, Bahrololoom M E and Zamani C (2011), *Surface Eng. and App. Electrochem*., **47**, 107-111.

Fujishima A and Honda K (1972), *Nature*, **238**, 37-38.

Feng Y W, Hong W, Hong X X, Zhang Y, Na Y X, Xia S S, Hui L Y, J Tao Z and Min W (2003) *J. Mol. Catalysis A*: *Chemical*, **202**, 305-311.

Folusho F, Ajayi, Kyu-Jung C, Kyoung-Yeol K, Mi-jin C and In S K (2009) *Int. J. Hydrogen Energy*, **34**, 110-114.

Fujinaka, Masahari V., Alexander A (1983) *J. Applied Physics*, **54**, 3582-3588.

Fujihara M, Ohishi N and Osa T (1977) *Nature*, **2**, 226-228.

Fujishima A and Honda K (1972) *Nature*, **238**, 37-38.

Garuthara R and Siripala W (2006) *J. Lumin.*, **121**, 173–178.

Getoff N and Popov P (2003) *Radiat, Phys. Chem*. **69(4)** 311-387.

Guillen E, Casanueva F, Anta J A, Vega-Poot A, Oskam G, Alcantara R, Fernandez-Lorenzo C and Martín-Calleja J (2008) *J. Photochemistry and Photobiology A: Chemistry*, **200,** 364-370.

Grimes CA, Su J, Guo L, Bao N (2011) *Nano Lett*., **11,** 1928-33.

Gonzalez M A S, Marigorta A M B, and Quintana J A P (2011), Review on hydrogen production technologies from solar energy, Int. Conference on Renewable Energies and Power Quality, Las palmas de gran canaria, Spain, 13th to 15th April.

Gupta M, Sharma V, shrivastava J, solanki A, singh A P, satsangi V R, dass S and Shrivastav R (2009), *Bull. Mater. Sci.*, **32**, 23–30.

Haga M A, Kobayashi K and Terada K (2007), *Coordination Chemistry Reviews*, **251**, 2688-2701.

Hou J, Wang Z, Jiao S, Zh H (2011), *J. Hazardous Mat.*, **192**, 1772-1779.

Han H, Theodore N D, Alford T L (2008) *J. Applied Physics*, **103**, 013708.

Haijian S, H Liu, Jun M, Xiangyu W, Bin W and Lei H (2008) *J. Hazardous Mat.*, **156**, 552–559.

Haixin C, Xiaojun L, Hao Z and Jinghong L (2010) *Electrochemistry Communication*, **12**, 483-487.

Honggang S, Wriliu F, Yanlu L, Xiufeng C, Pan L and Xian Z (2010) *J. Phys. Chem. C*., **114**, 3028-3036.

Huaming Y, Jing O, Aidong T, Yu X, Xianwei L, Xiaodan D and Yongmei Y (2006) *Materials Research Bulletin*, **41,** 1310-1318.

Hua C C and Teng H (2010) *Catalysis*, **271**, 1-8.

Hamedani H A, Allam N K, Garmestani H, Sayed M A (2011) *J. Phys. Chem.*, **115**, 13480–13486.

Itoh K and Bockris J O J (1984) *Appl. Physics*, **56**, 874-876.

Ingler B W and Khan U M S (2005) *Int. J. Hydrogen Ene.*, **30,** 821 -827.

Ishizuka S, Kato Shinya, Maruyame T and Akimoto K (2001) *J. Appl.Phys*., **40**, 2765-2768.

Jayewardena C, Hewaparakrama K P, Wijewardena D L A and Guruge H (1998) *Solar Energy Materials & Solar Cells* **56,** 29-33.

Jiaqing G, Dong Y, Juhong Z, Daimei C and Zhongyi J (2009) *Mat. Res. Bulletin*, **44**, 146.

Jongh P E, Vanmaekelbergh D, Kelly J J (1999) *Chem. Commun*., **DOI:** 10.1039/A901232J, 1069-1070.

Jeong S H, Park B N, Lee S B, Boo J H (2005) *Surface & Coatings Tech.*, **193**, 340– 344.

Junga S W, Parka J H, Seoa S W, Kima J H, Choib C J, Kimb H, Leec D K, Junga W S and Ahn K S (2011), *Molecular Crystals and Liquid Crystals*, 533-538.

Jyoko Y, SchwarzacherW (2001), *Electrochimical Acta*, **47**, 371–37.

Jiang J, Zhang J, Gu F, Shao W, Li C and Lu M (2011), *Particuology*, **9**, 222-227.

Koo C Y, Kim D, Jeong S and Moon J (2008), *J. of the Korean Physical Society*, **53**, 218-222.

Kronawitter C X , Vayssieres L , Shen S, Guo L, Wheeler D A , Zhang J Z, Antoun B R and Mao S S (2011), *Ene. Environ. Sci*., **4**, 3889-3899.

Kumar S G and Devi L G (2011), *J. Phys. Chem.* A, **115**, 13211–13241.

Kale S S, Rajaram S M, Ganesh T, Pawar B N and Sung-Hwan H (2009) *Current Applied Physics*, **9**, 384-389.
Kelly A N and Gibson L T (2006) *Int. J. Hydrogen Ene.*, **31**, 1658-1666.

Kim K, Debnath P C, Park D H, Kim S, and Lee S Y (2010) *Applied Physics Lett.*, **96**, 1-3.

Kitiyanan A, Ngamsinlapasathian S, Pavasupree S and Yoshikawa S (2005) *J. Solid State Chemistry,* **178,** 1044-1048.

Krishna Reddy J, Suresh G, Hymavathi C H, Durga Kumari V and Subrahmanyam M (2009) *Catalysis Today*, **141**, 89–93.

Kudo A, Yanagi H, Ueda K, Hosono H and Kawazoe H (1999), *Appl. Phys. Lett.*, **75**, 2851-2853.

Kumari S, Chaudhary Y S, Agnihotry S A, Tripathi C, Verma A, Chauhan D, Shrivastav R, Dass S, and Satsangi V R (2007) *Int. J. Hydrogen Ene.*, **32,** 1299-1302.

Liu J W, Chen G, Li Z H and Zhang Z G (2006) *J. Solid State Chemistry*, **179**, 3704-3708.

Liu Z, Guo B, Hong L and Jiang H (2005) *J. of Physics and Chem. of Solids,* **66,** 161–167.

Li-Yu L and Dae-Eun K (2009) *Thin Solid Films,* **517,** 1690-1700.

Ling Y, Wang G, Wheeler D A, Zhang J Z, and Li Y (2011) *J. American Chem. Society,* **11**, 2119–2125.

Li G, Wang T, Zhu Y, Zhang S, Mao C, Wu J, Jin B and Tian Y (2011) *App. Surface Sci.,* **257**, 6568-6572.

Logar M, Kocjan A and Dakskobler A (2011) *Mat. Res. Bull.*, **47**, 12-17.

Liu Y, Xie C, Li H, Chen H, Zou T, Zeng D (2011) *J. of Hazardous Mat.*, 196, 52-58.

Liu C J, Burghaus U, Besenbacher F and Wang Z L (2010) *Nano focus*, 4, 5517–5526.

Lin Y, Yuan G, Liu R, Zhou S, Sheehan S W, Wang D (2011) *Chem. Phys. Lett.*, 507, 209-215.

Li Y and Zhang J Z (2011) *Laser Photonics Reviews*, **36**, 48-55.

Lucatero S and Podlaha E J (2010) *J. of the Electrochemical Society*, **157**, 370-375.

Liu Z, Hou W, Pavaskar P, Aykol M and Cronin S B (2011) *Nano Lett.*, **11**, 1111–1116.

Li Q, Guo B, Yu J, Ran J, Zhang B, Yan H and Gong J R (2011) *American Chem. Soc*iety, **133**, 10878–10884.

Li J, Hui L, Jian Y and Wenfeng S (2010) *J. of Wuhan University of Technology-Mater. Sci. Ed. Dec.*, **25**, 919-923.

Lin C F, Wu C H and Onn Z N (2008) *J. of Hazardous Mat.*, **154**, 1033–1039.

Li H, Cheng C, Li X, Liu J, Guan C, Tay Y Y and Fan H J, (2012) *J. Phys. Chem. C*, **116**, 3802−3807.

Lee W W, Yi J, Kim S B, Kim Y H, Park H G, and Park W I (2011) *Cryst. Growth Des.*, **11**, 4927–4932.

Lee M, Kwak G, and Yong K (2011) *Appl. Mater. Interfaces*, **3**, 3350–3356.

Memar A, Ramli W, Daud W, Hosseini S, Eftekhari, Minggu L J (2010) *Solar Ene.*, **84**, 1538–1544.

Mona J, Mamgain H, Jejurikar S, Rawat R R, Ganesan V, Choudhary R J, Phase D M, Kale S N (2008) *App. Surface Sci.*, **254**, 4808-4812.

Murph S E H, Serkiz S M, Fox E B, Mercado H C, Sexton L and Siegfried M (2011) *Fluorine-Related Nanosci. with Ene. Appl*., Chapter **8**, 127–163.

Mukherji A , Marschall R , Tanksale A , Sun C , Smith S C , Lu G Q and Wang L (2011) *Adv. Funct. Mater*., **21**, 126–132.

Maria A, Panagiotis B, Nikolata S and Pangiotis L (2008) *Int. J. Hydrogen Ene.,* **33**, 5045-5051.

Martinez-Ruiz A and Alonso-Nunez G (2008) *Mat. Res. Bull.,* **43,** 1492-1496.

Miller L E, Rocheleau E R and Deng M X, (2003) *Int. J. Hydrogen Ene.,* **28,** 615-623.

Mishra R P, Shukla K P and Srivastava N O (2006) *Int. J. Hydrogen Ene.* **32,** 1677-1680.

Miyake H and Kozuka H (2005) *J. Phys. Chem. B,* **109**, 17951-17956.

Mohapatra S K, Misra M, Mahajan V K and Raja K S (2007) *J. Phys. Chem. C***, 111**, 8677-8685.

Muckopadhyay A K, Chakraborty A K, Chatterjee A P and Lahiri S K (1992) *Thin Solid Films*, **209**, 92-96.

Murphy A B, Barnes P R F, Randeniya L K, Plumb I C, Grey I E, Horne M D and Glasscocka J A (2006) *Int. J. Hydrogen Ene.,* **31,** 1999-2017.

Mathew M, Jayakrishnan R, Kumar P M, Kartha C S, and Vijayakumar K P (2006) *J. Applied physics*, **100**, 033504-033602.

Mao A, Shin K, Kim J K, Wang D H, Han G Y, and Park J H (2011), *Appl. Mater. Interfaces*, **3**, 1852–1858.

Nakaoka K and Ogura K (2002) *J. Electrochemical Soc.,* **149 (11)**, 775- 779.

Ohta T (2000), *Int. J. Hydrogen Ene.*, **25**, 287-293.

Ono T A, Noguch P, Inove Y, Kusunoki N, Matsushita T and Oyanagi H (1992) *Science*, **258**, 1335-1337.

Oscar K and Turner J A (1998) *Science*, **280**, 425-427.

Oszajca M F, McCall K L, Robertson N and Szacizowski K (2011) *J. Phys. Chem.,* **115**, 12187–12195.

Patra M K, Manot M., Singh V K, Siddaramana G G, Choudhry V S, Vadera S R and Kumar N (2009) *J. Luminescence,* **129**, 320.

Paulauskas I E, Katz J E, Jellison Jr. GE, Lewis N S and Boatner L A (2008) *Thin Solid Films*, **516,** 8175-8178.

Prakasam H E, Varghese O K, Maggie P, Gopal K M and Craig A G (2006) *Nanotechnology,* **17,** 4285.

Pattamatta A and Madnia C K (2009), *Int. J.of Heat and Mass Transfer*, **52**, 860-869.

Qin D D, Tao C L, Friesen S A, Wang T H, Varghese O K, Bao N Z, Yang Z Y, Mallouk T E and Grimes C A (2012), *Chem. Commun*., **48**, 729–731.

Qingyue C, Yong H and Ziqiang Z (2009) *Current Applied Physics*, **9**, 426-430.

Qin D D, Tao C L, In S I, Yang Z Y, Mallouk T E, Bao N and Grimes C A (2011), *Ene. Fuels*, **25**, 5257–5263.
Radecka M, Rekas M, Trenczek-Zajac A and Zakrzewska K (2008) *J. Power Sources,* **181**, 46-55.

Randeniya L K, Murphy A B and Plumb I C (2008) *J. Mater Sci*, **43**, 1389-1399.

Redon AM, Vigneron J, Heindl R, Sella C, Martine C and Dalbera J P (1981) *Solar Cells*, **3**, 179-186.
Riess I, Feldman I, Zvi R (2004) *Solid State Ionics*, **175**, 375-378.

Riha S C, Fredrick S J, Sambur J B, Liu Y, Prieto A L and Parkinson B A (2011), *App. Mat. and Interfaces*, **3**, 58–66.

Saikia D, Saikia P K, Gogoi P K, Saikia P (2011) *J. Nanomat. Biostruct.*, **6**, 589-597.

Shinar R and Kennedy J H (1982) *Sol. Ene. Matter.*, **6**, 323-335.

Shukla P K, Karn R K, Singh A K and Srivastava O N (2002) *Int. J. Hydrogen Ene.*, **27**, 135–141.

Souhila B, Rabah B, Mohamed T and Aissa B (2009) *Ene. Conversion and Management*, **50,** 62–68.

Stuart L (2001) *J. Phys. Chem.* B, **105**, 6281-6294.

Sharma R, Das P P, Misra M, Mahajan V, Bock J P, Trigwell S , Biris A S and Mazumder M K (2009) *Nanotechnology*, **20,** 075704.

Shen Q, Liu Y, Xu J, Meng C and Liu X (2010) *J. Royal Society of Chem.*, **46**, 5701–5703.

Sun-kim M, Rajaram S M, Oh-Shim J, Ganesh T, Byung W C and Sung-Hwan H (2009) *Current Applied Physics*, **9**, 492-495.

Sharma V, Kumar P, Shrivastava J, Solanki A, Satangi V R, Dass S, Shrivastav R (2011) *Int. J. Hydrogen Ene.*, **36**, 4280-4290.

Sun Y, Murphy C J, Reyes- Gil K R, Enrique A R G, Lilly J P and Raftery D (2008) *Int. J. Hydrogen Ene.*, **33**, 5967-5974.

Sahaym U and Norton M G (2008) *J. Mater Sci.*, **43**, 5395–5429.

Sharma P, Kumar P, Solanki A, Shrivastav R, Dass S and Satsangi V R (2010) *Int. J. of hydrogen ene.*, **35**, 10883-10889.

Sun B, Hao Y, Guo F, Cao Y, Zhang Y, Li Y, and Dongsheng Xu (2012) *J. Phys. Chem. C*, **116**, 1395–1400.

Su J, Guo L, Bao N and Grimes C A (2011) *Nano Lett*., **11**, 1928–1933.

Shinagawa T, Watase S and Izaki M (2011) *Cryst. Growth Des.*, **11**, 5533–5539.

Tokarz A, Wieczorek P, Lis A K and Morgiel J (2010) J. Microsc., **237(3)**, 456-60.

Tiginyanu I M, Lupan O, Ursaki V V, Chow L and Enachi M (2011) Comprehensive Semiconductor Sci. and Tech., **3**, 396-479.

Tafalla D and Salvador P (1989) *J. Electroancrl Chem.*, **270,** 285-295.

Tomas E, Neil P, Jan S, Felix E, Gerrit B, and Anders H (2008) *J. Chem.Phys*., **111**, 15137-15140.

Tsay Tie-C, Cheng Chi-H, Tung Ting-Y, Tuan Hsing-W and Lin Kwei-C (2008) *Thin Solid Films*, **517**, 1032-1036.
Tong H, Ouyang S, Bi Y, Umezawa N, Oshikiri M and Ye J (2012) *Adv. Mater*., **24**, 229–251.

Vercelli B and Zotti G (2012) *J. Phys. Chem. C*, **116**, 2033–2039.

Wang L C, De Tacconi N R, Chenthamarakshan C R, Rajeshwar K and Tao M. (2007) *Thin Solid Films*, **515**, 3090-3095.

Wang M, Hahn S H, Kim E J, Kim J S, Kim S, Park C and Koo Kee-K (2008) *Thin Solid Films*, **516**, 8599-8603.

Wang B, Li C, Hirabayashia D and Suzuki K (2010) *Int. J. Hydrogen Ene.*, **35**, 3306-3312.

Wenfeng S (2007) *Sci. and Tech. of Advanced Mat.*, **8**, 76-81.

Wenjun L, Tao Y, Yaoming W, Zhaosheng L, Jinhua Y and Zhigang Z (2007) *J. Phys. D: Appl. Phys*., **40**, 1091-1096.

Wijesundera R.P, Hidaka M, Koga K, Sakai M and Siripala W, (2006) *Thin Solid Films*, **500,** 241-246.

Wirth J, Monturet S, Klamroth T and Saalfrank P (2011) *J. EPL*, **93**, 68001.

Wong K K, Ng A, Chen X Y, Ng Y H, Leung Y H, Ho K H, Djurisic A B, Ng A M C, Chan W K, Yu L and Phillips D L (2012) Appl. Mater. Interfaces dx.doi.org/10.1021/am201424d.

Xiaoyan G, Xiaomin L, Xiangdong G, Xiliang H and Fuwei Z (2009) *Mat. Chem. and Physics*, **114**, 920-925.

Xinjian F, Thomas J, James I B, Gopal K M, Oomman K V and Craig A G (2010) *Nano Lett.*, **10**, 948-952.

Xunyu Y, Abraham W, Gongming W, Alissa S, Roberl C F, Fang Q, Jin Z Z and Vat L (2009) *Nano Lett.*, **9**, 2331-2336.

Yasuyoshi S, Hiroaki N, Kenji S and Akihiko K (2009) *J. Phys. Chem*. C, **113**, 17536-17542.

Yokoyamaa D, Minegishia T, Maedaa K, Katayamaa M, Kubotaa J, Yamadab A, Konagaib M and Domen K (2010) *Electrochemistry Communications*, **12**, 851-853.

Yoon K H, Choi W J and Kang D H (2000) *Thin Solid Films*, **372**, 250-256.

Yanga H, Yana J, Lua Z, Chenga X and Tanga Y (2009) *J. of Alloys and Compounds*, **476**, 715–719.

Yue B, Li Q, Iwai H, Kako T and Ye J (2011) *Sci. Technol. Adv. Mater*., **12**, 1-7.

Zaban A, Aruna S T, Tirosh S, Gregg B A and Mastai Y (2000) *J. Phys. Chem. B*, **104**, 4130- 4133.

Zeyan W, Baibiao H, Xiaoyan Q, Xiaoyang Z, Peng W, Jiyong W, Jie Z, Xiangyang J, Haixia L, Zhenhua X, Hefeng C, Xiaoning W and Zhaoke Z (2009) *Phys. Chem*, **63**, 130-132.

Zhou G and Yang J C (2003) *Applied Surface Science*, **210**, 165-170.

Zhonghai Z, Hossainb F and Takahashi T (2010) *Int. J. Hydrogen Ene.* , **36**, 13481–13487.

Zeferino R S, Flores M B and Pal U (2011) *J. Applied Physics*, **109**, 014308.

Zhang S, Sakai R, Abe T, Iyoda T, Norimatsu T, and Nagai K (2011) *Applied Mat. Interfaces*, **3**, 1902–1909.

Zhang Y M, Hu Q, Ge Y, Lu J, He Z, Chen L, and Yin (2010) *Chem. Eur. J*., **16**, 6243-6250.